Gaia Data Release 2

D. Katz, P. Sartoretti, M. Cropper, P. Panuzzo, G. M. Seabroke, Y. Viala, K. Benson, R. Blomme, Gérard Jasniewicz, A. Jean-Antoine, et al.

D. Katz, P. Sartoretti, M. Cropper, P. Panuzzo, G. M. Seabroke, et al.. Gaia Data Release 2: Properties and validation of the radial velocities. Astronomy and Astrophysics - A&A, 2019, 622, pp.A205. 10.1051/0004-6361/201833273 . hal-01868258

A&A 622, A205 (2019)
https://doi.org/10.1051/0004-6361/201833273

Gaia Data Release 2

Astronomy & Astrophysics
Special issue

Gaia Data Release 2

Properties and validation of the radial velocities

D. Katz[1], P. Sartoretti[1], M. Cropper[2], P. Panuzzo[1], G. M. Seabroke[2], Y. Viala[1], K. Benson[2], R. Blomme[3], G. Jasniewicz[4], A. Jean-Antoine[5], H. Huckle[2], M. Smith[2], S. Baker[2], F. Crifo[1], Y. Damerdji[6,7], M. David[8], C. Dolding[2], Y. Frémat[3], E. Gosset[7,9], A. Guerrier[10], L. P. Guy[11], R. Haigron[1], K. Janßen[12], O. Marchal[1], G. Plum[1], C. Soubiran[13], F. Thévenin[14], M. Ajaj[1], C. Allende Prieto[2,15,16], C. Babusiaux[1,17], S. Boudreault[2,18], L. Chemin[13,19], C. Delle Luche[1,10], C. Fabre[20], A. Gueguen[1,21], N. C. Hambly[22], Y. Lasne[5], F. Meynadier[1,23], F. Pailler[5], C. Panem[5], F. Royer[1], G. Tauran[5], C. Zurbach[4], T. Zwitter[24], F. Arenou[1], D. Bossini[25], J. Gerssen[12], A. Gómez[1], V. Lemaitre[5], N. Leclerc[1], T. Morel[7], U. Munari[26], C. Turon[1], A. Vallenari[25], and M. Žerjal[24,27]

(Affiliations can be found after the references)

Received 20 April 2018 / Accepted 12 December 2018

ABSTRACT

Context. For *Gaia* DR2, 280 million spectra collected by the Radial Velocity Spectrometer instrument on board *Gaia* were processed, and median radial velocities were derived for 9.8 million sources brighter than $G_{\rm RVS} = 12$ mag.

Aims. This paper describes the validation and properties of the median radial velocities published in *Gaia* DR2.

Methods. Quality tests and filters were applied to select those of the 9.8 million radial velocities that have the quality to be published in *Gaia* DR2. The accuracy of the selected sample was assessed with respect to ground-based catalogues. Its precision was estimated using both ground-based catalogues and the distribution of the *Gaia* radial velocity uncertainties.

Results. *Gaia* DR2 contains median radial velocities for 7 224 631 stars, with $T_{\rm eff}$ in the range [3550, 6900] K, which successfully passed the quality tests. The published median radial velocities provide a full-sky coverage and are complete with respect to the astrometric data to within 77.2% (for $G \leq 12.5$ mag). The median radial velocity residuals with respect to the ground-based surveys vary from one catalogue to another, but do not exceed a few 100 m s^{-1}. In addition, the *Gaia* radial velocities show a positive trend as a function of magnitude, which starts around $G_{\rm RVS} \sim 9$ mag and reaches about +500 m s^{-1} at $G_{\rm RVS} = 11.75$ mag. The origin of the trend is under investigation, with the aim to correct for it in *Gaia* DR3. The overall precision, estimated from the median of the *Gaia* radial velocity uncertainties, is 1.05 km s^{-1}. The radial velocity precision is a function of many parameters, in particular, the magnitude and effective temperature. For bright stars, $G_{\rm RVS} \in [4, 8]$ mag, the precision, estimated using the full dataset, is in the range 220–350 m s^{-1}, which is about three to five times more precise than the pre-launch specification of 1 km s^{-1}. At the faint end, $G_{\rm RVS} = 11.75$ mag, the precisions for $T_{\rm eff} = 5000$ and 6500 K are 1.4 and 3.7 km s^{-1}, respectively.

Key words. techniques: spectroscopic – techniques: radial velocities – catalogs – surveys

1. Introduction

The ESA *Gaia* mission (Gaia Collaboration 2016a) was launched from the Kourou space centre on 19 December 2013. It took about four weeks for the satellite to reach its operational orbit around the second Lagrange point (L2) of the Sun-Earth system. Following the commissioning phase, the nominal mission began on 25 July 2014, initially for a five-year period, which has recently been granted a first extension by 1.5 yr[1]. *Gaia* continuously scans the celestial sphere with its two telescopes and its three instruments: the astrometric instrument, a spectrophotometer, and a spectrograph with a medium resolving power, the Radial Velocity Spectrometer (RVS, Cropper et al. 2018). The data collected are daily transmitted to Earth, when the satellite is in contact with one of the ground-based antennas. Once received on the ground, the data are processed by the *Gaia* Data Processing and Analysis Consortium (DPAC). The consortium publishes the products of the processing in successive data releases. The first of these, *Gaia* DR1 (Gaia Collaboration 2016b), was issued on 16 September 2016, and the second, *Gaia* DR2 (Gaia Collaboration 2018a), on 25 April 2018.

Each new *Gaia* data release includes new products. One of the novelties of *Gaia* DR2 is the publication of the median radial velocities that are extracted from the RVS spectra. The RVS collects spectra down to $G_{\rm RVS} = 16.2$ mag. Because of the modest exposure time per CCD of 4.42 s, however, the signal-to-noise ratio (S/N) of the spectra of the faintest stars is very low. The derivation of the radial velocities of the faintest stars will require combining the entire spectroscopic information collected for each source over the full mission. For *Gaia* DR2, 280 million spectra that were recorded during the first 22 months of the nominal mission were processed, and median radial velocities were obtained for 9.8 million stars down to magnitude $G_{\rm RVS} = 12$ mag. The spectroscopic pipeline and the processing of the spectra are described in detail in a companion paper (Sartoretti et al. 2018).

---

[1] The current cold gas fuel supplies of *Gaia* would allow an extension of the nominal mission by five years.

In the past 15 yr, spectroscopic surveys have delivered radial velocities, as well as stellar parameters and abundances for large stellar samples. Examples are the Geneva-Copenhagen-Survey (Nordström et al. 2004) with ∼17 000 stars, SEGUE (Yanny et al. 2009) with ∼240 000 stars, APOGEE (Holtzman et al. 2015) with ∼150 000 stars, APOGEE-2 (Majewski et al. 2017; Abolfathi et al. 2018) with ∼263 000 stars, RAVE (Steinmetz et al. 2006; Kunder et al. 2017) with ∼460 000 stars in DR5, the *Gaia*-ESO-Survey (Gilmore et al. 2012; Sacco et al. 2014; Jackson et al. 2015) with ∼50 000 stars in DR3, LAMOST (Cui et al. 2012; Zhao et al. 2012) with ∼5.3 million stars in DR5, and GALAH (Buder et al. 2018; Zwitter et al. 2018) with ∼340 000 stars in DR2. In continuity of these large surveys, *Gaia* DR2 contains median radial velocities for 7 224 631 stars with $T_{\rm eff}$ in the range [3550, 6900] K that are distributed throughout the entire celestial sphere.

This paper is devoted to the description and validation of the median radial velocities published in *Gaia* DR2. After a short summary of the main characteristics of the RVS instrument (Sect. 2) and a brief overview of the spectroscopic processing pipeline (Sect. 3), Sect. 4 presents the filters that were applied after the completion of the processing to select the radial velocities with the quality to be published in *Gaia* DR2. Section 5 describes the properties of the published radial velocities.

2. Radial velocity spectrometer

The RVS is described in detail in Cropper et al. (2018). Here we provide a very brief description of the main characteristics of the instrument.

The RVS is an integral field spectrograph with a medium resolving power, $R = \lambda/\Delta\lambda = 11\ 500$, that observes in the near-infrared at $\lambda \in [845, 872]$ nm. Like the astrometric and photometric instruments, the RVS is illuminated by the two *Gaia* telescopes. The spectra are recorded in a block of 12 CCDs (3 in the direction of the scan, times 4 in the direction perpendicular to the scan) located at the edge of the *Gaia* focal plane. When a source crosses one of the two fields of view (hereafter referred to as transit), 3 spectra are recorded, that is, one per CCD in the scan direction. The exposure time per CCD is 4.42 s. On average, the RVS is expected to record 40 transits per source during the five years of the nominal mission.

Gaia is continuously spinning and scanning the sky with a six-hour period. The CCDs are therefore operated in time-delay integration (TDI) mode, that is, the charges are transferred from column to column at high frequency in order to follow the sources while they cross the focal plane. In order to minimise both the telemetry budget and the electronic noise, elongated windows are read around the spectra and transmitted to the ground. The remaining pixels are flushed in the readout register and discarded. At the start of the nominal mission, the windows were 1260 pixels long (i.e. in the sense of the spectral dispersion, which is also the orientation of the scan) and 10 pixels wide. The length of the windows was increased to 1296 pixels in June 2015 to allow for a better measure of the background light. The on-board software allocates windows to sources down to $G_{\rm RVS} = 16.2$ mag, which is the limiting magnitude of the RVS.

The RVS is an integral field spectrograph and therefore disperses the light of all the sources that are contained in its two fields of view, with the consequence that the spectra of very close neighbours will overlap. In this case, to avoid transmitting the pixels twice, the on-board software can decide to truncate the windows in the direction perpendicular to the dispersion, that is, allocating fewer than 10 pixels to the window width. If the conflict does not extend on the full length of the spectrum, the truncation will only be applied to the appropriate portion of the spectrum, resulting in a non-rectangular window. For *Gaia* DR2, only rectangular windows were processed. The specific treatments required by non-rectangular windows are planned for *Gaia* DR3.

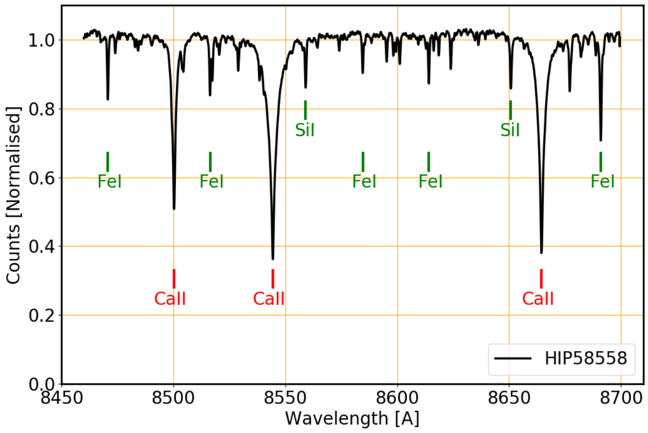

Fig. 1. RVS spectrum of the star HIP 58558.

During commissioning, it was found that the level of stray light was higher than expected. Although the spectroscopic pipeline subtracts the scattered light, the noise in the spectra is increased. This affects faint stars more strongly, in particular those close to the RVS limiting magnitude. The origin, properties, on-board mitigation, and consequences of the stray light are described in Cropper et al. (2018). The treatment of the scattered light by the spectroscopic pipeline is presented in Sartoretti et al. (2018).

In *Gaia* DR2, median radial velocities are published for stars with $T_{\rm eff}$ in the interval [3550, 6900] K. In this temperature range, the RVS spectra are dominated by a triplet of the ionised calcium. The wavelength range also contains weaker neutral metallic lines of iron, silicon, or titanium, for instance. As an example, Fig. 1 presents the RVS spectrum of the star HIP 58558: $T_{\rm eff} = 5477$ K, $\log g = 4.34$, and [Fe/H] = 0.02 dex (Adibekyan et al. 2012). Below about 3400 K, the RVS spectra develop strong molecular bands. In A and B spectral types, the P13–P17 hydrogen Paschen lines become the dominant spectral features. As discussed in Sect. 4, the radial velocities of cool and hot stars, that is, stars beyond [3550, 6900] K, will be published in a future *Gaia* release.

3. Spectroscopic pipeline

3.1. Overview

The *Gaia* spectroscopic processing pipeline is described in detail in Sartoretti et al. (2018). In this section, we provide a brief overview of its functionalities.

The spectroscopic pipeline is in charge of four main tasks:

1. Calibrating the RVS instrument. The pipeline developed for *Gaia* DR2 calibrates the electronic bias, the read-out noise, the wavelengths, and the $G_{\rm RVS}$ magnitude zero-point. For the other RVS characteristics, the pipeline relies either on pre-launch or off-line calibrations.
2. Reducing and cleaning the spectra. This includes in particular subtracting the electronic bias and the stray light, discarding spectra degraded by CCD cosmetic defects or saturation, applying the wavelength calibration, removing

the cosmic rays, normalising the continuum, deriving the internal $G_{\rm RVS}$ magnitude, and selecting a template to derive the radial velocity.

3. Measuring the radial velocities per transit. For each star and for each transit one (or two, in the case of a double star) radial velocity is measured. Each radial velocity is derived by a series of modules that compare the three RVS spectra collected per transit to one (or several) template(s) shifted step by step in radial velocity, from -1000 to $+1000$ km s^{-1}. This workflow is hereafter referred to as single-transit analysis (STA).
4. Combining the information of the successive transits. For each source, the radial velocities derived in successive transits are grouped into a time series. The radial velocities published in *Gaia* DR2 are the medians of these time series (see Sect. 5.1.1 for more details). Statistical properties of the time series are also calculated and are used as variability and quality indicators. In addition, for each source, all recorded spectra are shifted to rest frame and combined. The combined spectra are then examined in order to detect possible emission lines. This set of tasks is hereafter referred to as multiple-transit analysis (MTA*)*.

3.2. Selection of the templates

The proper selection of the templates and their similarities with the observed spectra plays an important role in the quality of the radial velocities that are derived (see Sects. 4 and 5). Because of its impact on the performance, we present this specific task of the pipeline here. A more detailed description is provided in Sartoretti et al. (2018).

About 15% of the stars processed for *Gaia* DR2 had known ground-based atmospheric parameters. When available, this information was used to select the closest template in a library of several thousand synthetic spectra. When the parameters were unknown, a dedicated software module, *determineAP*, chose the template by comparison of the RVS spectrum to a set a synthetic spectra. For *Gaia* DR2, 280 million spectra were processed. The data volume was too large to compare 85% of the RVS spectra to the full library of synthetic spectra. To keep the processing load reasonable, *determineAP* had to select the templates in a sub-grid restricted to 28 synthetic spectra. The sub-grid contains 18 different temperatures, ranging from 3100 to 35 000 K, two metallicities: solar for all the temperatures and [Fe/H] = −1.5 dex for nine of them, and a single choice of surface gravity for most temperatures. In STA, a single template is used per star, that is, the same for all the transits.

3.3. $G_{\rm RVS}$ and G magnitudes

Different measures of the $G_{\rm RVS}$ magnitude are either produced or used by the pipeline and in this paper. They are defined below:

- The on-board $G_{\rm RVS}$ ($G_{\rm RVS}^{\rm on-board}$) is derived by the *Gaia* on-board software.
- The external $G_{\rm RVS}$ ($G_{\rm RVS}^{\rm ext}$) is calculated from ground-based photometric catalogues using colour–colour transformations. When no ground-based photometry is available, the on-board $G_{\rm RVS}^{\rm on-board}$ is adopted. $G_{\rm RVS}^{\rm ext}$ is the magnitude used to define the limiting magnitude of *Gaia* DR2: $G_{\rm RVS}^{\rm ext} \leq 12$ mag.
- The internal $G_{\rm RVS}$ ($G_{\rm RVS}^{\rm int}$) is measured by the spectroscopic pipeline (Sartoretti et al. 2018) from the RVS spectra. For the faint stars, the accuracy and precision of $G_{\rm RVS}^{\rm int}$ are limited by the basic modelling of the stray light in *Gaia* DR2. A more elaborated calibration of the stray light is being developed for *Gaia* DR3.

In Sect. 5.1 we assess the completeness as a function of the G magnitude, which is the *Gaia* broadband magnitude measured from the astrometric windows (Riello et al. 2018; Evans et al. 2018). The colour of a typical un-reddened G2V star is $G - G_{\rm RVS} \sim 0.65$ mag (Jordi et al. 2010).

4. Selecting radial velocities for publication in *Gaia* DR2

For *Gaia* DR2, the spectroscopic pipeline has processed 280 million spectra and produced radial velocities for 9.8 million stars without pre-selection on spectral type or colour indices and for a very broad range of S/N. The pipeline includes validation functionalities, described in Sartoretti et al. (2018), which can autonomously identify and reject problematic data such as negative total spectrum flux or nearby duplicated transits. These diagnostics are usually meant to detect issues at spectrum or transit level. They do not consider the global properties of the data (known a posteriori) and the potential outliers. Therefore, following the completion of the processing, an off-line validation campaign was conducted on the full 9.8 million star sample to assess its characteristics and identify the stars that did not have the quality to be published in *Gaia* DR2. This resulted in the list of filters described below.

Large coordinate uncertainties. The right ascensions and declinations (computed by the *Gaia* astrometric pipeline, see Lindegren et al. 2018) are used to derive the coordinates of the sources in the RVS fields of view, which are then used to calibrate the spectra in wavelength. The uncertainties on the coordinates of the sources are therefore propagated to the wavelengths of the spectra and in fine to the radial velocities. In *Gaia* DR2, the mean precision on the source positions is 0.03 mas, which represents a very minor contribution to the radial velocity error budget of ∼4.3 m s^{-1}. Of course, a small fraction of the stars presents much larger astrometric uncertainties. The radial velocities of ∼8000 stars with a quadratic sum of the uncertainties on the right ascension and on the declination, that is, $\sqrt{\epsilon_\alpha^2 + \epsilon_\delta^2}$, larger than 100 mas (corresponding to ∼14.5 km s^{-1}), were discarded from *Gaia* DR2.

Faint stars. For *Gaia* DR2, stars brighter than $G_{\rm RVS}^{\rm ext} = 12$ mag were processed by the spectroscopic pipeline. The selection was performed using the external $G_{\rm RVS}^{\rm ext}$ magnitude (see Sect. 3.3). The spectroscopic pipeline also derives an internal $G_{\rm RVS}^{\rm int}$ magnitude based on the flux contained in the RVS spectrum between 846 and 870 nm. It was considered that the ∼165 000 stars with an internal $G_{\rm RVS}^{\rm int}$ magnitude equal to or fainter than 14 mag did not contain enough signal per spectrum to yield a good enough velocity in *Gaia* DR2.

Ambiguous transits. The STA workflow produces a boolean quality flag, *isAmbiguous*[2], which identifies the radial velocities that look suspicious in a specific transit. In validation, the ratio of the number of ambiguous transits over the total number transits was examined for each source. The distribution on the celestial sphere of this new quality indicator shows a very specific pattern. While in most of the sky, the mode of its distribution peaks at 0, in a few specific areas it peaks at 1 (i.e. peaks

---

[2] A radial velocity derivation module will flag a transit radial velocity as *isAmbiguous* if two or more of the three velocities derived for the three RVS CCDs (crossed during that transit) are too discrepant. A detailed description of the derivation of the *isAmbiguous* flag is provided in Sect. 7.7 of Sartoretti et al. (2018).

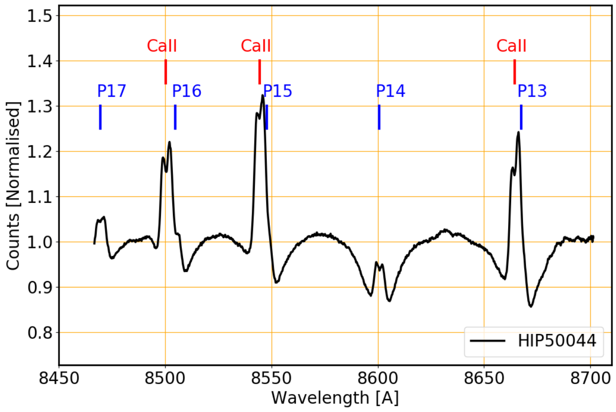

Fig. 2. RVS spectrum of the Be star HIP 55044, the Ca II and the Paschen lines are both in emission.

at 100% of ambiguous transits per source). This behaviour appears to be partly related to the overestimation of the external $G^{\mathrm{ext}}_{\mathrm{RVS}}$ magnitude in some specific areas, allowing some faint stars to enter the spectroscopic processing. The radial velocities of the ∼611 000 stars with 100% ambiguous transits were excluded from *Gaia* DR2. The two filters on faint stars and ambiguous transits show some overlap, both rejecting stars whose signal in the RVS window is too low. Because they consider different quantities, they are also complementary, however. One possibly identifies a suspicious star that the other could have missed.

Large radial velocity uncertainties. The distribution of unfiltered radial velocity uncertainties peaks between 1 and 2 km s^{-1} and shows either an extended tail or a broad small amplitude secondary peak (depending on the location on the sky). The extended tail/econdary peak includes a mix of stars whose signal is too weak to be processed in *Gaia* DR2, large amplitude variables, and undetected binary or multiple systems. In all these cases, the median radial velocity published in *Gaia* DR2 would not be a reliable estimate of the source or system radial velocity. The median radial velocities of the ∼1.6 million stars with a radial velocity uncertainty larger or equal to 20 km s^{-1} were discarded from *Gaia* DR2.

Suspected double-line spectroscopic binaries. The STA workflow includes a software module that detects the spectra that present double-line patterns and derives their two radial velocities. The multi-instrument modelling and publication of binary systems is planned for *Gaia* DR3. Therefore, in *Gaia* DR2, the ∼113 000 stars for which more than 10% of their transits are flagged as double-line patterns were considered as potential double-line spectroscopic binaries (SB2), and their median radial velocities were removed from *Gaia* DR2.

Suspected emission-line stars. The MTA workflow includes a software module that detects emission-line stars. The library of spectra used for *Gaia* DR2 does not contain emission-line templates. The comparison of an emission-line star with an inappropriate absorption-line template can produce systematic radial velocity shifts of several hundred km s^{-1}. The radial velocities of ∼7000 stars that were identified as potentially emission-line stars were excluded from *Gaia* DR2. Figure 2 shows the RVS spectrum of the star HIP 55044 as an example. It was detected as an emission-line star by the *MTA* workflow. It is classified in the literature as a Be star (Houk & Cowley 1975).

Cool stars. In the RVS domain, the spectra of late-M stars are dominated by TiO molecular bands. The spectra show steep slopes, and because of the narrow RVS wavelength range, the pseudo-continuum is usually not visible on the side of the shortest wavelengths. For these stars, the radial velocity precision is more sensitive than for other spectral types to the treatment of the continuum as well as to the choice of the template. Tests conducted during the validation phase showed that the radial velocity performance was significantly lower for the stars that were processed using templates with effective temperatures of 3500 K or lower. The radial velocities of ∼747 000 stars processed with a cold-star template were removed from *Gaia* DR2. The spectroscopic pipeline will be upgraded to process late M-type stars and publish their radial velocities in a future *Gaia* data release.

Hot stars. The validation phase showed that the 28 synthetic spectra available to the module *determineAP* to select the templates (see Sect. 3.2), and in particular the single choice of gravity per effective temperature, were insufficient for hot stars. In early-F and A-type stars, the Paschen lines are significantly pressure sensitive and become stronger with decreasing surface gravity. Three of the Paschen lines, that is, P13, P15, and P16, are blended with the Ca II lines. The profiles of the blended lines change with surface gravity, and as a consequence, the centroids of the lines are shifted. This can produce a systematic bias on the radial velocity of several km s^{-1} if it is derived with the inappropriate template. The systematic error can be amplified if the star shows a significant projected rotational velocity, which will modify the "narrow" profile of the Ca II lines more strongly than the broader profiles of the Paschen lines. Therefore, the ∼996 000 radial velocities derived using a template with an effective temperature of 7000 K or higher were excluded from *Gaia* DR2.

Figure 3 illustrates the sensitivity of the Ca II-Paschen blends to surface gravity and rotational velocity. HIP 66525 (top) has $T_{\mathrm{eff}} \sim 8000$ K and $\log g \sim 4.6$ (Kordopatis et al. 2013), while HIP 91843 (bottom) has $T_{\mathrm{eff}} \sim 8100$ K and $\log g \sim 3.2$ (derived from 2MASS photometry). The Paschen lines are clearly stronger in the latter than in the former. Moreover, in HIP 91843, the depth of the Ca II lines is reduced by the projected rotational velocity broadening.

In *Gaia* DR3 and following releases, the atmospheric parameters should be derived by elaborated analysis of the *Gaia* spectrophotometric data, and for the brightest stars, of the RVS spectra. The spectroscopic pipeline will also be upgraded to derive the rotational velocities. The radial velocities of hot stars will be published when the precisions on the atmospheric parameters and on the rotational velocities will allow processing them with the appropriate template and blend profiles.

High-velocity stars. Of the more than seven million stars that successfully passed the above filters, the absolute radial velocities of 613 were higher than or equal to 500 km s^{-1}. Because this sample of high-velocity stars is very small compared to the full sample, it can easily be significantly contaminated by outliers. For example, a hypothetical rate of one undetected outlier in 10 000 stars (generating an incorrect random uniformly distributed radial velocity) times the about seven million total valid radial velocities would produce about 350 false high-velocity stars, that is, stars with $|V_{\mathrm{R}}| \geq 500$ km s^{-1}. As a consequence, particular attention was paid to them. Their combined spectra (see Sect. 3) were visually examined one by one, and the proper locations of their Ca II lines was checked. Of the 613 stars, 216 were considered as valid high-velocity stars, and the median radial velocity of the 397 others were removed from *Gaia* DR2. Another 14 stars were rejected by astrometric and/or photometric filters, so that *Gaia* DR2 contains 202 stars with

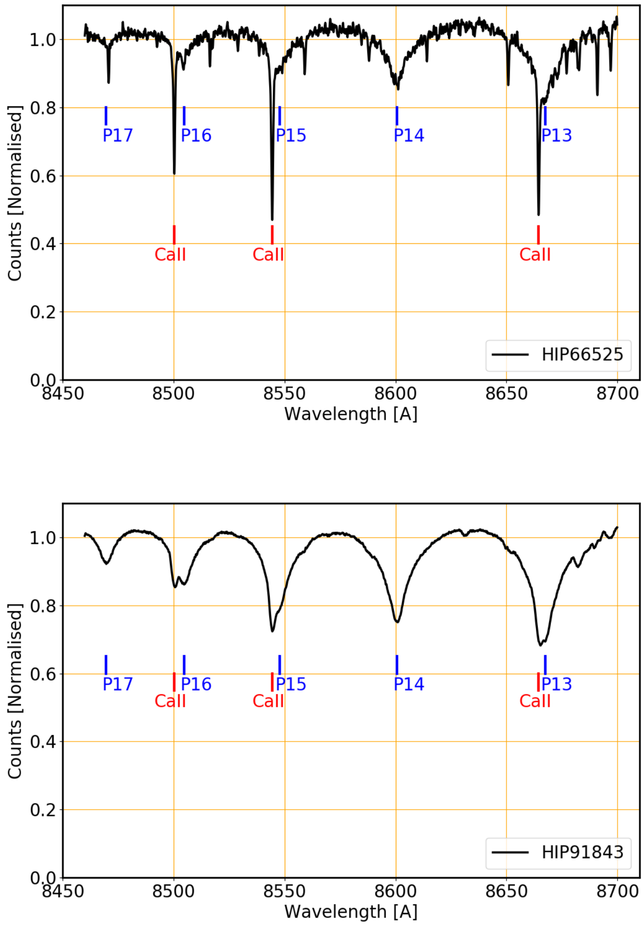

Fig. 3. RVS spectra of HIP 66525 (*top panel*) and HIP 91843 (*bottom panel*).

$|V_R| \geq 500$ km s^{-1}. A posteriori, it is possible to assess the contamination rate before cleaning. It decreased with the absolute value of the radial velocity and was ~90% in the range [950, 1000] km s^{-1} and ~20% in the range [500, 550] km s^{-1}. The number of stars increased too fast with decreasing absolute value of the velocity to extend the systematic visual inspection to slower stars. It is therefore important, when working with *Gaia* DR2 high-velocity stars, to take into account that an additional quality filter has been applied to stars faster than 500 km s^{-1}, resulting in different selection functions for the stars below and above this value.

Many stars that failed to pass one criterion in the end missed several of them. In total, 2.6 million median radial velocities were discarded for *Gaia* DR2, mostly by the above spectroscopic filters, but some also by other DPAC filters based on photometric or astrometric criteria (Gaia Collaboration 2018a; Lindegren et al. 2018; Evans et al. 2018; Arenou et al. 2018).

5. *Gaia* DR2 radial velocity catalogue

This section describes the content of the *Gaia* DR2 radial velocity catalogue, that is, the products and their properties (Sect. 5.1). It presents the assessment of the *Gaia* DR2 radial velocity accuracy (Sect. 5.2) and precision (Sect. 5.3).

5.1. Catalogue content

Gaia DR2 contains median radial velocities for 7 224 631 stars as well as their radial velocity uncertainties, number of transits, and template parameters (effective temperature, surface gravity, and metallicity). The spectroscopic fields published in *Gaia* DR2 are listed in Table 1.

Table 1. Spectroscopic content of *Gaia* DR2.

Field	Units	DB column name
Median radial velocity	km s^{-1}	radial_velocity
Radial velocity uncertainty	km s^{-1}	radial_velocity_error
Number of transits	transits	rv_nb_transits
Template temperature	K	rv_template_teff
Template surface gravity	dex	rv_template_logg
Template metallicity	dex	rv_template_fe_h

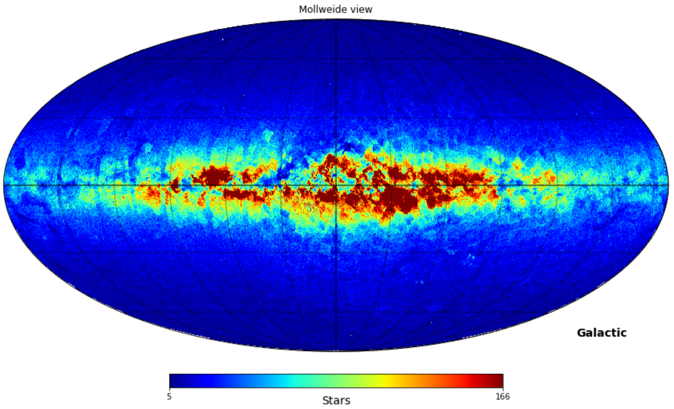

Fig. 4. Distribution on the sky of the 7 224 631 stars with a radial velocity in *Gaia* DR2. The projection is in Galactic coordinates. The Galactic centre is in the middle of the figure and the Galactic longitudes increase to the left. The pixel size is about 0.2 square degree (healpix level 7).

The spectroscopic catalogue covers the full sky. Figure 4 shows the distribution in Galactic coordinates of the stars with a radial velocity in *Gaia* DR2. The vast majority of the stars belong to the Milky Way, but some bright members of the Large and Small Magellanic Clouds are also part of this release.

The external $G^{\rm ext}_{\rm RVS}$, used in *Gaia* DR2 to define the limiting magnitude of the spectroscopic pipeline, is mainly calculated from ground-based photometry (Sect. 3.3). Different catalogues were used in different areas of the sky and with different colour–colour relations. This led to small variations of the $G^{\rm ext}_{\rm RVS}$ zero-point and therefore of the limiting magnitude of the processing, as a function of celestial coordinates. The variations are visible in the star counts as small amplitude patterns of one to a few degrees in size.

Figure 5 shows the *G*-magnitude distribution of the stars with a radial velocity in *Gaia* DR2. For the release, the spectroscopic pipeline has processed stars down to $G^{\rm ext}_{\rm RVS} = 12$ mag. Because a majority of stars are fainter in *G* than in $G_{\rm RVS}$ (for an un-reddened G2V star, $G - G_{\rm RVS} = 0.65$ mag), however, the mode of the *G*-magnitude distribution is located in the range $G \in [12.5, 13]$ mag. The minimum value, first quartile, median, third quartile, and maximum value (not visible in the figure) of the distribution is $G \sim 1.9, 11.7, 12.5, 13.0,$ and 18.3 mag, respectively.

Figure 6 (top) shows the completeness of the *Gaia* DR2 radial velocities with respect to the full *Gaia* DR2 catalogue as a function of *G*-magnitude. The completeness increases smoothly from $G \sim 4$ to $G \sim 11.5$ mag. The steep decrease for the faint

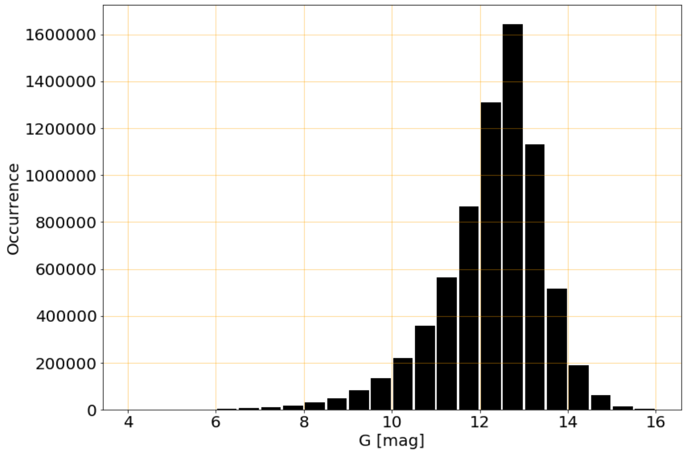

Fig. 5. *G*-magnitude distribution of the stars with a radial velocity published in *Gaia* DR2.

stars is a consequence of the limiting magnitude of *Gaia* DR2 processing: $G^{\mathrm{ext}}_{\mathrm{RVS}} = 12$ mag. The sharp cut-off at $G \sim 4$ mag is due to the saturation of the core of the RVS spectra, which are then discarded by the spectroscopic pipeline. The completeness for $G \leq 12.5$ is 77.2%.

Figure 6 (bottom) shows the completeness with respect to the *Gaia* DR2 catalogue as a function of Galactic coordinates for the stars with $G \leq 12.5$ mag. At first order, the completeness is driven by the projected stellar density. In dense areas, the conflicts between RVS windows are more frequent, leading to a higher probability of the windows to be truncated and therefore not processed by the pipeline. As a consequence, the completeness is lower in the directions of the Galactic bulge and in the Galactic disc and rapidly increases farther away from the Galactic plane. A second effect, still related to stellar density, plays a role in the completeness. The number of spectra that can be simultaneously read per RVS CCDs is limited (Cropper et al. 2018). The threshold corresponds to a stellar density of about 36 000 sources per square degree. As a consequence, some spectra are not read in a given transit in dense areas. This effect is partly mitigated by the repeated scans of the sky. A source that is not recorded in one transit might be in the following ones. The completeness is therefore expected to increase with the successive data releases as a longer time range will be processed, for instance, 60 months for the full nominal mission versus 22 months for *Gaia* DR2.

5.1.1. Median radial velocity

The radial velocity published in *Gaia* DR2 is the median of the radial velocities derived per transit. Some observations were not used for the calculation of the median:

- Truncated windows (caused by the overlap with the window of another star) were not processed for *Gaia* DR2 and therefore had no transit V_{R} derived (for that transit).
- Transits for which a spectrum was flagged as double-line spectroscopic binaries (SB2) were excluded from the calculation of the median.

A minimum of two eligible (i.e. non-truncated, non-SB2) transits were required to derive the median radial velocity of a star. The radial velocities of ~1.6 million sources with a single eligible transit were not published in *Gaia* DR2.

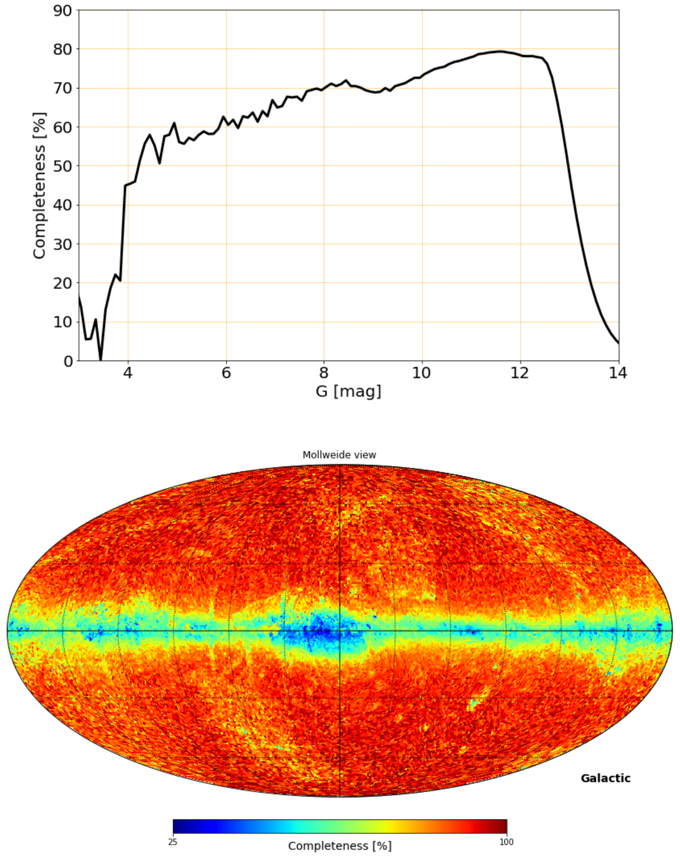

Fig. 6. *Top panel*: completeness with respect to the full *Gaia* DR2 catalogue as a function of *G* magnitude. *Bottom panel*: completeness with respect to the *Gaia* DR2 catalogue for the stars with $G \leq 12.5$ mag as a function of galactic coordinates. The Galactic centre is in the middle of the figure and the Galactic longitudes increase to the left. The pixel size is ~0.8 square degree (healpix level 6).

Figure 7 (top) shows the map of the medians of the *Gaia* DR2 radial velocities, $\tilde{V}_{\mathrm{R}}$, as a function of Galactic coordinates. The medians are calculated over healpix level 7 pixels of about 0.2 square degree each (the same area as the star count map: Fig. 4). Figure 7 (bottom) presents the face-on view map of the medians of the *Gaia* DR2 radial velocities of the Galactic disc stars for sources located within ±1 kpc of the Galactic mid-plane. The stars in the face-on map were also selected on the basis of their relative parallax uncertainty: $\sigma_{\varpi}/\varpi \leq 20\%$. The medians of the *Gaia* DR2 radial velocities are calculated over cells of 200 pc × 200 pc. Both maps show the line-of-sight-projected differential rotation of the stars of the Galaxy, as observed from the Sun. The Large and Small Magellanic Clouds also stand out clearly in the top part of Fig. 7 around $(l, b) \sim (-80°, -33°)$ and $(-57°, -44°)$, respectively.

5.1.2. Radial velocity uncertainty

The radial velocity uncertainty is calculated as the uncertainty on the median of the transit radial velocities quadratically summed with a constant term of 0.11 km s^{-1}, which represents the current calibration noise floor:

$$\epsilon_{V_{\mathrm{R}}} = \left[\left(\sqrt{\frac{\pi}{2N}}\sigma_{V^{\mathrm{t}}_{\mathrm{R}}}\right)^2 + 0.11^2\right]^{0.5}, \qquad (1)$$

where N is the number of eligible transits used to derive the median radial velocity, $\sigma_{V^{\mathrm{t}}_{\mathrm{R}}} = \sqrt{\frac{1}{N-1}\sum_{i=1}^{N}\left(V^{\mathrm{t}}_{\mathrm{R}}(i) - \overline{V^{\mathrm{t}}_{\mathrm{R}}}\right)^2}$ the

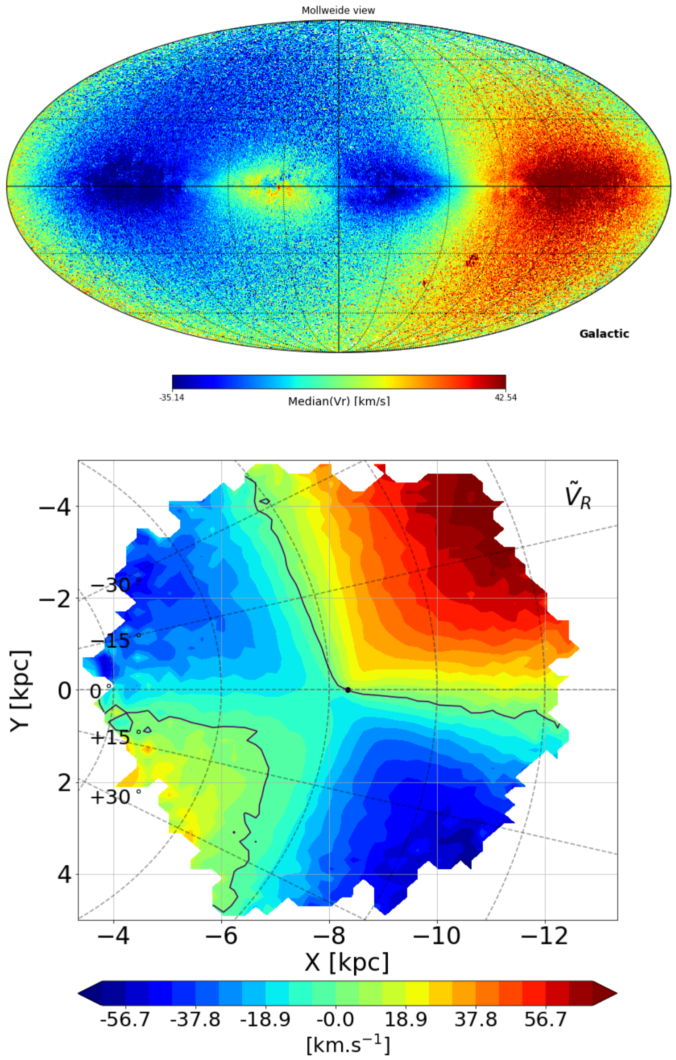

Fig. 7. *Top panel*: map of the medians of the *Gaia* DR2 radial velocities as a function of Galactic coordinates. The Galactic centre is in the middle of the figure and the Galactic longitudes increase to the left. The pixel size is ~0.2 square degree (healpix level 7). *Bottom panel*: face-on view map of the medians (over cells of 200 pc × 200 pc) of the *Gaia* DR2 radial velocities, $\tilde{V}_{\rm R}$, for the Galactic disc as seen from the north Galactic pole. The Galactic azimuths increase clockwise. They are labelled from −30° to +30° on the left of the map. The Sun is represented by a black dot, located at $X = -8.34$ kpc (Reid et al. 2014) and $Y = 0$ kpc. The Galactic centre is located on the left side. The Milky Way rotates clockwise. The Galactic longitudes are defined counter-clockwise (around the Sun). The iso-velocity contour $\tilde{V}_{\rm R} = 0$ is pointed out as black lines. The map has been calculated using 5 020 596 stars, selected in a 2 kpc horizontal layer centred on the Galactic mid-plane.

standard deviation of the eligible transit radial velocities, $V_{\rm R}^{\rm t}(i)$ the ith transit radial velocity of the time series, and $\overline{V_{\rm R}^{\rm t}}$ the mean radial velocity.

Figure 8 shows the distribution of the radial velocity uncertainties. The first quartile, median, and third quartile of the distribution are 0.55, 1.05, and 2.08 km s^{-1}, respectively.

The radial velocity uncertainty relies on the standard deviation of the time series of transit radial velocities. As described in the next section (Sect. 5.1.3), some time series are made of a few transits, in which cases the standard deviations and therefore the radial velocity uncertainties are less precise than for larger numbers of transits.

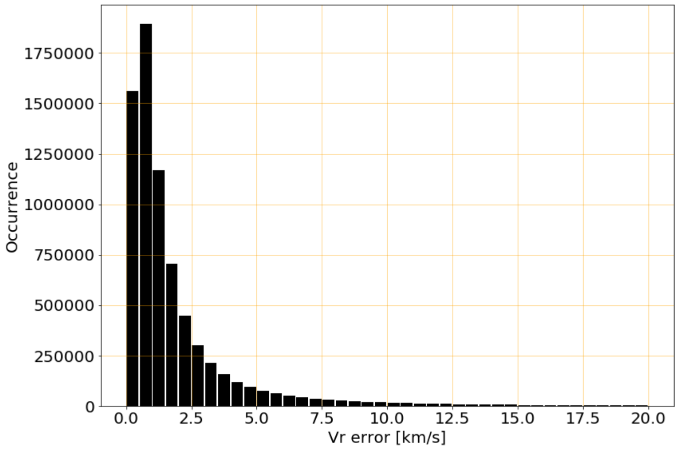

Fig. 8. Distribution of the radial velocity uncertainties.

5.1.3. Number of transits

The number of transits published in *Gaia* DR2 is the number of eligible transits used to compute the median radial velocity. Figure 9 (top) shows the distribution of the number of transits. It ranges from 2 (by construction) to 201, with a median number of 7.

The main driver of the number of observations for a source is the satellite scan law, which defines how many times a specific area of the sky has been monitored. During the first 28 days of the nominal mission, *Gaia* was in ecliptic pole scanning law (EPSL) and observed each ecliptic pole with each telescope every six hours (the spin period of the satellite). The stars with many transits are stars that lie close to the ecliptic poles that have been monitored repeatedly during the 28 days of EPSL. The second factor that defines the number of transits is the stellar density. In dense areas, the stars are closer and the probability of conflict (i.e. overlap) between RVS windows is higher. For *Gaia* DR2, overlapped windows have not been processed, and as a consequence, the mean number of transits is lower in dense areas. It should be noted that the satellite scans have different orientations at different transits. Because of the very elongated geometry of the windows, it is not systematic that a star overlaps with the same neighbour at each transit. Therefore, the stellar density first affects the number of transits and then the completeness (which is also affected, as shown in Sect. 5.1). Figure 9 (bottom) shows the distribution on the sky (Galactic coordinates) of the median number of transits per ~0.2 square degree pixel.

5.1.4. Parameters of the template

The transit radial velocities are derived by comparison (cross-correlation or minimum distance methods, see Sartoretti et al. 2018) with a synthetic spectrum that is referred to as template. The spectroscopic pipeline has two ways to select a template. If the parameters of the star are contained in the compilation of ground-based stellar parameters that are used by the pipeline (see Sartoretti et al. 2018), they are used to select the closest template in a library of 5256 spectra. Otherwise, the template is chosen by a dedicated module, *determineAP*, from a smaller set of 28 templates (see Sect. 3.2). Of the 7 224 631 stars, ~18% had their templates selected using the ground-based compilation. Appendix A details the distributions of the parameters of the templates.

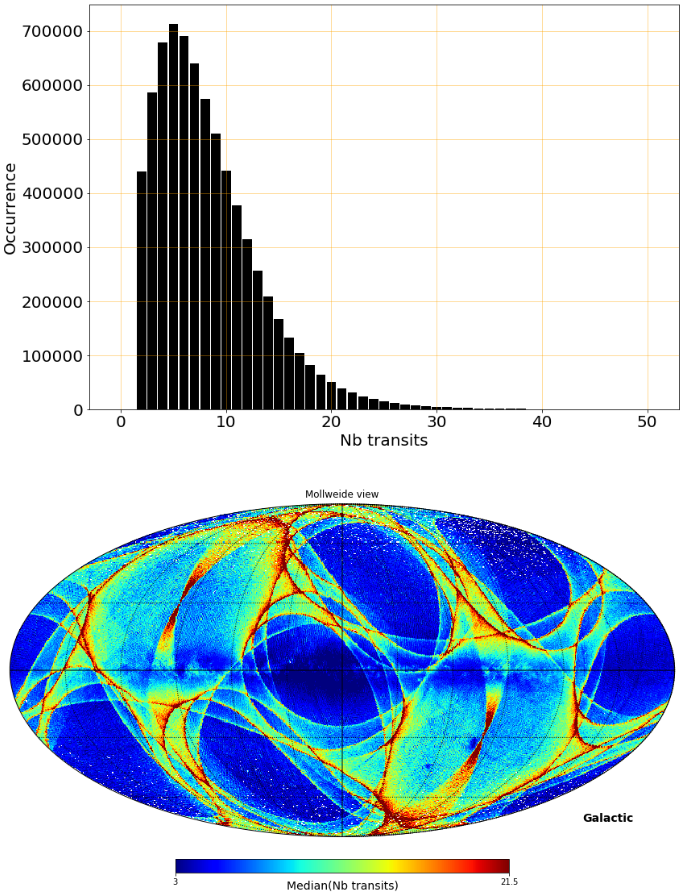

Fig. 9. *Top panel*: distribution of the number of transits per star used to derive the median radial velocity. The full distribution extends to 201 transits. The 1053 stars (0.015% of the total) with more than 50 transits are not shown in the histogram. *Bottom panel*: distribution of the median number of transits as a function of galactic coordinates. The Galactic Centre is in the middle of the figure and the galactic longitudes increase to the left. The pixel size is about 0.2 square degree (healpix level 7).

The template parameters are published in the second *Gaia* release in order to inform the users about the synthetic spectra that were used to derive the radial velocities. They are not meant to be used as an estimate of the stellar atmospheric parameters for any other purpose. It should be noted that *Gaia* DR2 contains effective temperature estimates, derived from G, $G_{\rm BP}$, and $G_{\rm RP}$ photometry, for about 160 million stars with $T_{\rm eff} \in [3000, 10\,000]$ K and brighter than $G = 17$ mag (Andrae et al. 2018).

5.2. Radial velocity accuracy

The accuracy is the systematic difference between the measured values and the true values. Unfortunately, the true values of the radial velocities of the *Gaia* DR2 stars are not known. Therefore, five ground-based catalogues[3] are used as proxy: CU6GB (Soubiran et al. 2018), SIM (Makarov & Unwin 2015), RAVE (Kunder et al. 2017), APOGEE (Abolfathi et al. 2018), and the *Gaia*-ESO-Survey (GES; Gilmore et al. 2012). In each case, only a subset of these catalogues has been selected, which is made of stars that show no radial velocity variability. Because our GES validation sub-sample is small, it was only used to assess the accuracy as a function of the $G_{\rm RVS}$ magnitude.

The limitation of the comparison to external catalogues is that they can, of course, also be affected by their own biases. Therefore, when a systematic difference is observed between *Gaia* DR2 and a catalogue, it could come from the former, the latter, or both. Using several external catalogues is meant to help (assuming that they do not share some systematic(s)). It should be noted that even if the true accuracy is difficult to assess from the comparison of different catalogues, it is of interest to know their relative differences, for combining data from these catalogues or comparing results obtained independently with them, for instance.

CU6GB (Soubiran et al. 2018) is a ground-based radial velocity catalogue produced by the *Gaia* DPAC. The zero-point of the radial velocities of the CU6GB catalogue (i.e. its accuracy) has been assessed by comparing measured radial velocities of asteroids to celestial mechanics predictions. The zero-point of CU6GB is 38 ± 5 m s^{-1}.

As an estimator of accuracy, we use the median of the radial velocity residuals, $V_{\rm R}^{\rm res}$ (i.e. *Gaia* DR2 minus ground-based catalogue). The lower and upper 1σ uncertainties on the estimate of the accuracy are calculated as

$$\epsilon_{\rm acc}^{\rm low} = \sqrt{\frac{\pi}{2N_{V_{\rm R}^{\rm res}}}}(\tilde{V}_{\rm R}^{\rm res} - {\rm Per}(V_{\rm R}^{\rm res}, 15.85)), \tag{2}$$

$$\epsilon_{\rm acc}^{\rm upp} = \sqrt{\frac{\pi}{2N_{V_{\rm R}^{\rm res}}}}({\rm Per}(V_{\rm R}^{\rm res}, 84.15) - \tilde{V}_{\rm R}^{\rm res}), \tag{3}$$

respectively, where $N_{V_{\rm R}^{\rm res}}$ is the number of radial velocity residuals, $\tilde{V}_{\rm R}^{\rm res}$ is the median of the radial velocity residuals, and ${\rm Per}(V_{\rm R}^{\rm res}, 15.85)$ and ${\rm Per}(V_{\rm R}^{\rm res}, 84.15)$ are the 15.85th and 84.15th percentiles of the distribution of radial velocity residuals. In the following sections, the accuracy is studied as a function of different parameters (e.g. $G_{\rm RVS}^{\rm ext}$, $G_{\rm RVS}^{\rm int}$, $T_{\rm eff}$, and $\log g$). The comparison samples are therefore divided by bins of the considered quantities. In these cases, a minimum of 20 stars per bin is required to calculate the median of the radial velocity residuals.

Table 2 presents the median radial velocity residuals derived for the five ground-based catalogues. *Gaia* DR2 shows a small 2.4σ level offset of -12 m s^{-1} with respect to CU6GB. The CU6GB stars brighter than or equal to $G_{\rm RVS}^{\rm ext} = 9$ mag that showed no variability were used in the wavelength calibration procedure to set the wavelength zero-point of each configuration: that is, field-of-view/CCD/trending epoch (Sartoretti et al. 2018). It is a good sanity check for the pipeline that neither the wavelength calibration nor the subsequent modules modified the global radial velocity zero-point defined by the CU6GB catalogue significantly. *Gaia* DR2 shows a positive global offset of about +200 to +300 m s^{-1} with respect to the SIM, RAVE, APOGEE, and GES stars. As discussed in the following sections, the origin of these offsets varies partially from one catalogue to another, however.

5.2.1. Accuracy versus number of transits

Figure 10 shows the median radial velocity residuals as a function of the number of eligible transits. In general, the accuracy is not expected to improve or vary with the number of measures. In

---

[3] Arenou et al. (2018) also compared the *Gaia* DR2 radial velocities to the first GALAH data release (Kos et al. 2017; Martell et al. 2017). The second GALAH data release (Buder et al. 2018; Zwitter et al. 2018) was published after the completion of the validation of *Gaia* DR2.

Table 2. Median radial velocity residuals derived from the comparison of *Gaia* DR2 with ground-based catalogues.

Catalogue	Median $V_R^{\rm res}$ (km s^{-1})	$N_{\rm stars}$
CU6GB	−0.012 −0.005/+0.005	4083
SIM	+0.264 −0.015/+0.014	640
RAVE	+0.295 −0.013/+0.013	9127
APOGEE	+0.233 −0.011/+0.013	8124
GES	+0.236 −0.043/+0.049	2120

Notes. $N_{\rm stars}$ (Col. 3) is the number of stars selected to calculate the median residuals.

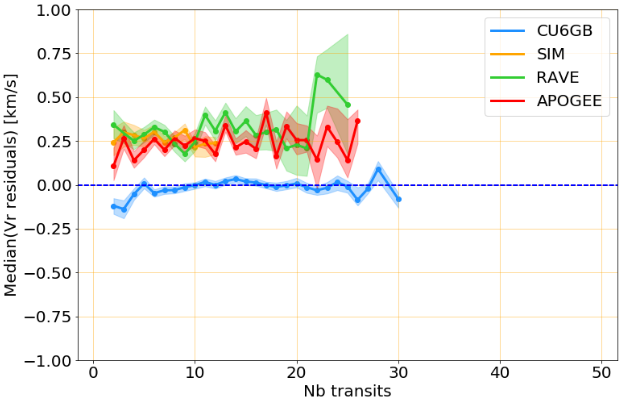

Fig. 10. Median radial velocity residuals as a function of the number of transits. The lower and upper 1σ uncertainties on the measures of the medians are represented as shaded areas.

Gaia DR2, the number of transits is highly correlated with the location of the stars on the sky, however (bottom part of Fig. 9). Therefore, potential spatial biases might have been propagated to the number of transits. *Gaia* DR2 shows no significant trend or discontinuity with respect to the CU6GB (which covers the full celestial sphere), SIM, or APOGEE datasets. The median of the residuals with respect to the RAVE dataset shows a 1–2σ upward jump over the range 22–24 transits. This feature is not present in the other datasets and remains compatible with statistical fluctuations. The accuracy as a function of the position on the sky is directly assessed in Sect. 5.2.7.

5.2.2. Accuracy versus $G_{\rm RVS}$

Figure 11 (top) shows the median radial velocity residuals as a function of the external $G_{\rm RVS}^{\rm ext}$ magnitude. Over the magnitude range [7, 9] mag, *Gaia* DR2 shows no significant offset nor trend with respect to the CU6GB or APOGEE stars, and it shows a nearly constant offset (similar to the global offset reported in Sect. 5.2) with respect to SIM and RAVE stars. Beyond $G_{\rm RVS}^{\rm ext} \sim$ 9–10 mag, the *Gaia* DR2 velocities exhibit an increasing positive offset with respect to all the catalogues for fainter stars, reaching about ~500 m s^{-1} at $G_{\rm RVS}^{\rm ext} \sim 11.75$. The trend is also visible in the median of the residuals as a function of the internal $G_{\rm RVS}^{\rm int}$ magnitude, which is derived from the flux recorded in the RVS windows (middle part of Fig. 11).

Each validation catalogue contains a mix of stars of different temperatures, gravities, and metallicities, whose proportion could change with magnitude. In order to check that the observed trend at faint magnitude was not caused by a differential effect between dwarfs and giants whose proportion could be function of magnitude, for example, a sub-sample of 3220 solar metallicity giant stars was selected that fulfilled the criteria $T_{\rm eff}$ in [4500, 5000] K, log g in [2.3, 3.0], and [Fe/H] in [−0.3, 0.3] dex. Figure 11 (bottom) presents the median radial velocity residuals as a function of the external $G_{\rm RVS}^{\rm ext}$ for the giant star sub-sample. As for the full validation sample, at magnitude brighter than $G_{\rm RVS}^{\rm ext} \sim 9$ (APOGEE) or 10 mag (RAVE), the offset is constant. At fainter magnitude, the median residuals exhibit a positive gradient with magnitude.

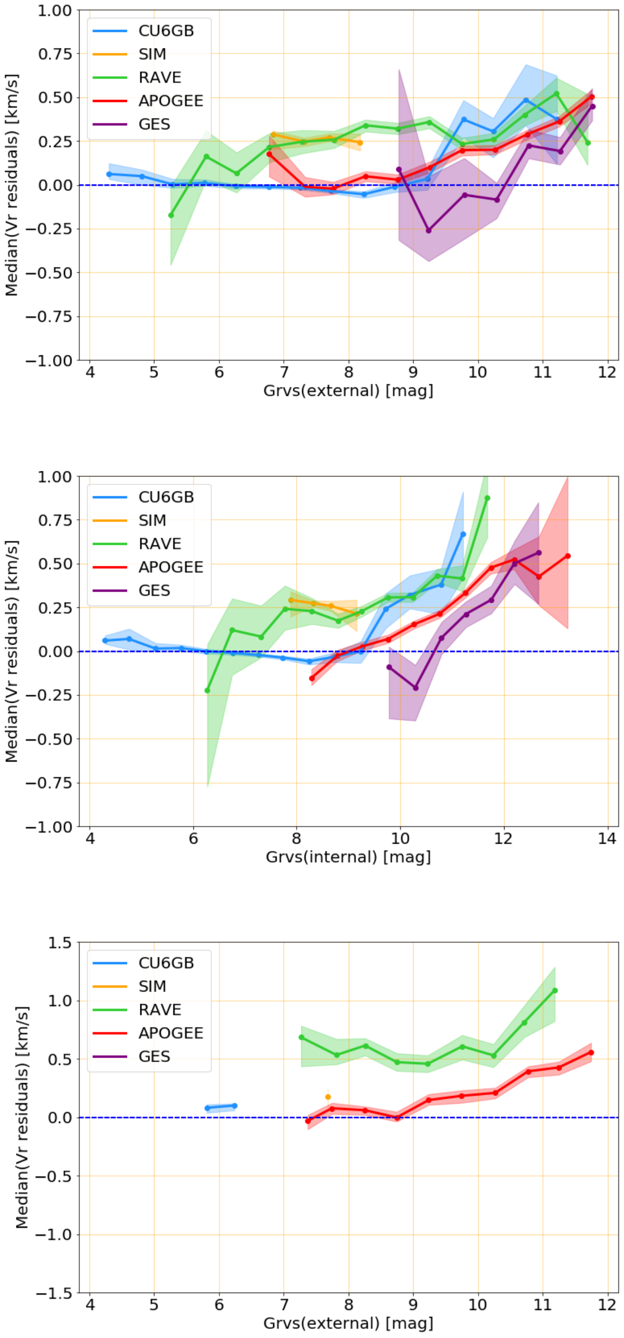

Fig. 11. *Top panel*: median radial velocity residuals as a function of the external $G_{\rm RVS}^{\rm ext}$ magnitude. *Middle panel*: median radial velocity residuals as a function of the internal $G_{\rm RVS}^{\rm int}$ magnitude. *Bottom panel*: median radial velocity residuals as a function of the external $G_{\rm RVS}^{\rm ext}$ magnitude for a subset of giant stars. The lower and upper 1σ uncertainties on the measures of the medians are represented as shaded areas.

Fig. 12. *Top panels*: median radial velocity residuals as a function of the effective temperature of the stars (*left panel*) and of the templates (*right panel*). *Middle panels*: median radial velocity residuals as a function of the surface gravity of the stars (*left panel*) and of the templates (*right panel*). *Bottom panels*: median radial velocity residuals as a function of the metallicity of the stars (*left panel*) and of the templates (*right panel*). The lower and upper 1σ uncertainties on the measures of the medians are represented as shaded areas.

The same trend is observed with all the validation catalogues for both the external and internal G_{RVS} magnitudes and for the full sample as well as for a subset of similar giant stars. The probability is therefore high that the effect is in the *Gaia* DR2 data. The origin of the trend is under investigation. The first lead explored was the charge transfer inefficiency (CTI), but this hypothesis has been dismissed (see Appendix B). The calibrations of the wavelengths and of the instrumental profile are now scrutinised to assess if they could play a role in the trend. The aim is to understand, model, and correct for the trend in *Gaia* DR3.

It should be noted that while the SIM and RAVE validation samples already present an offset for bright stars (which increases further for RAVE faint stars), APOGEE bright stars present little offset. The global offset between *Gaia* DR2 and APOGEE reported in Sect. 5.2 is mainly due to the prevalence of faint stars in this validation sample, while there is a global offset with respect to RAVE and SIM stars. Table 3 presents the median radial velocity residuals for the subsets of stars, from the validation catalogues, that are brighter than $G_{\mathrm{RVS}}^{\mathrm{ext}} = 9$ mag.

5.2.3. Accuracy versus temperature

Figure 12 (top) presents the median radial velocity residuals as a function of the stellar effective temperature[4] (left) and as a function of the template effective temperature (right). Both

---

[4] The effective temperatures, surface gravities, and metallicities used here and in the following sections come from the compilation of ground-based catalogues used by the spectroscopic pipeline (Sartoretti et al. 2018). Stellar parameters from different catalogues were usually derived with different methods and therefore show some heterogeneity in their zero-points and scales.

Table 3. Median radial velocity residuals derived from the comparison of *Gaia* DR2 with stars from the ground-based catalogues brighter than $G^{\mathrm{ext}}_{\mathrm{RVS}} = 9$ mag.

Catalogue	Median $V^{\mathrm{res}}_{\mathrm{R}}$ (km s^{-1})	N_{stars}
CU6GB	-0.017 $-0.005/+0.005$	3805
SIM	$+0.264$ $-0.015/+0.014$	640
RAVE	$+0.282$ $-0.019/+0.019$	3838
APOGEE	$+0.024$ $-0.015/+0.017$	1141
GES	-0.184 $-0.418/+0.254$	63

Notes. N_{stars} (Col. 3) is the number of stars selected to calculate the median residuals.

the CU6GB and the RAVE validation samples show a drop in median residuals by about 500 m s^{-1} for cool stars, from 4750–4500 to 4000 K. Over the same temperature range, the APOGEE sample exhibits flat residuals. Beyond ~5500 K, the median residuals of the APOGEE sample show a smooth decrease of about 200 m s^{-1}.

At about 4500 K (where the CU6GB and RAVE curves show an inflection), the RVS spectra are dominated by the Ca II triplet. The morphology of the spectra evolves smoothly with effective temperature. There is no sudden change in the RVS spectra that would produce the inflection observed in the two curves (but not in the APOGEE spectra).

Similar radial velocity offsets between M and K and hotter spectral types have been reported in the literature when measures from different spectrographs were compared. In particular, Soubiran et al. (2018) observed jumps of approximately −100 m s^{-1} and approximately +300 m s^{-1} around J–$K \sim 0.75$ mag for Sophie (Perruchot et al. 2008) minus Harps (Queloz et al. 2001; Mayor et al. 2003) and Sophie minus Elodie (Baranne et al. 1996) radial velocities, respectively. The authors hypothesised that the jumps might be caused by the use of different masks with different radial velocity zero-points in the pipelines of the three instruments.

5.2.4. Accuracy versus gravity

Figure 12 (middle) presents the median radial velocity residuals as a function of the stellar surface gravity (left) and as a function of the template surface gravity (right). The main feature is a smooth decrease in median residuals of the *Gaia* DR2 data versus RAVE by about 700 m s^{-1} between $\log g \sim 2.5$ and $\log g \sim 1$. The effect is not seen in the other validation samples, in particular APOGEE, which also extends to low gravities.

5.2.5. Accuracy versus metallicity

Figure 12 (bottom) presents the median radial velocity residuals as a function of the stellar metallicity (left) and as a function of the template metallicity (right). The median residuals of the *Gaia* DR2 versus RAVE velocities show a positive trend with metallicity that reaches ~750 m s^{-1} for the most metal-rich sources. On the metal-poor side, the CU6GB sample shows a negative offset of about −500 m s^{-1} for the stars whose velocity was calculated with templates that have a metallicity of −1.5 dex. The APOGEE validation sample shows no significant trend with metallicity.

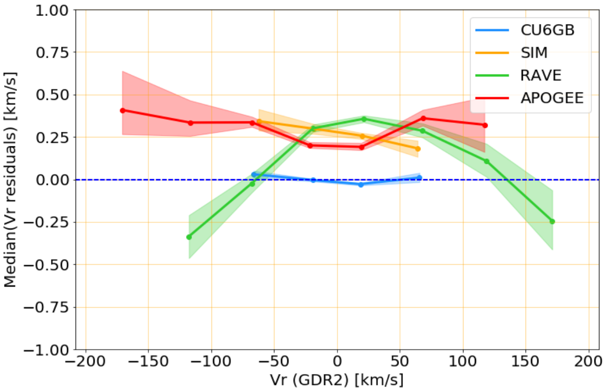

Fig. 13. Median radial velocity residuals as a function of the *Gaia* DR2 radial velocity. The lower and upper 1σ uncertainties on the measures of the medians are represented as shaded areas.

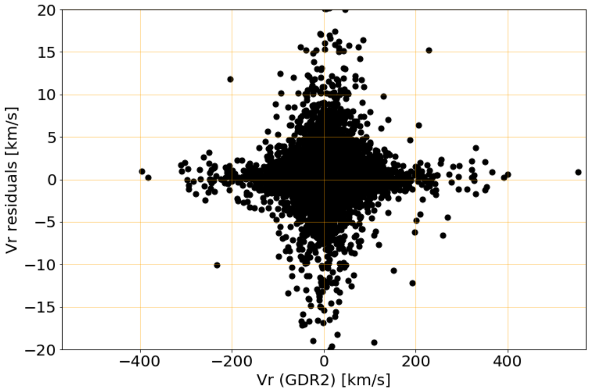

Fig. 14. Individual radial velocity residuals as a function of the *Gaia* DR2 radial velocity for 24 063 validation stars. Thirty-one validation stars with an absolute value of the radial velocity residual higher than 20 km s^{-1} are not displayed. The dots extend to higher residuals at low absolute velocities than at higher absolute velocities. This visual effect arises because low absolute velocities are much more densely populated than higher velocities, and therefore the wings of the residual distribution are probed to much higher values.

5.2.6. Accuracy versus velocity

Figure 13 presents the median radial velocity residuals as a function of the stellar velocity. The residuals of the *Gaia* DR2 versus RAVE velocities decrease by about 600–700 m s^{-1} from +25 to −125 km s^{-1} and show a symmetric behaviour at positive velocities. The small number of high-velocity stars in our validation datasets prevents us from deriving precise median residuals outside [−175, +175] km s^{-1}, whereas the pipeline derives radial velocities in the range [−1000, +1000] km s^{-1}. The individual radial velocity residuals (Fig. 14) provide a view on a broader velocity interval. The individual residuals do not show any strong offset or trend over the interval [−400, 400] km s^{-1}. The fastest validation star has a radial velocity of 552.6 km s^{-1} in our RAVE list and 553.5 km s^{-1} in *Gaia* DR2. As described in Sect. 4, the combined spectra of the stars with radial velocities $|V_{\mathrm{R}}| \geq 500$ km s^{-1} were visually inspected one by one, and those that we considered as false high-velocity stars were discarded from *Gaia* DR2.

5.2.7. Accuracy versus sky coordinates

Figure 15 presents the sky map in Galactic coordinates of the median radial velocity residuals per pixel of ~54 square

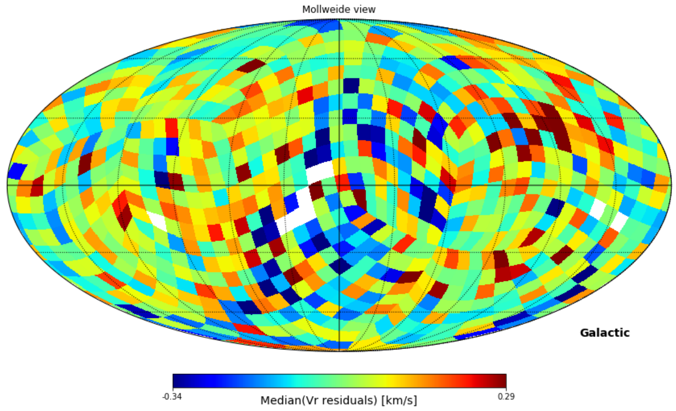

Fig. 15. Sky map in Galactic coordinates of the median radial velocity residuals per pixel of ~54 square degrees (healpix level 3). The Galactic centre is in the middle of the figure and the Galactic longitudes increase to the left.

degrees (healpix level 3). To increase the number of validation stars, the five ground-based catalogues presented in Sect. 5.2 have been complemented with 5820 stars from the Extended HIPPARCOS Compilation (XHIP; Anderson & Francis 2012). Nonetheless, for a few pixels, the minimum number of stars required to calculate the median, lowered here to 5 stars per pixel, was not reached. Those pixels appear in white on the map. To produce the map, the validation datasets have been corrected for their respective median radial velocity residuals (see Table 2) and then combined. This explains why the distribution of median radial velocity residuals is roughly centred on zero. The 2nd and 98th percentiles of the distribution are −0.34 and +0.29 km s^{-1}, respectively, while the extrema are −0.81 and +0.64 km s^{-1}.

The XHIP radial velocities come from the compilation of 47 different sources (Anderson & Francis 2012) with different radial velocity zero-points. This makes the median of the residuals of *Gaia* DR2 versus XHIP more difficult to interpret, and it was therefore not used in the previous sections to assess the accuracy of *Gaia* DR2. The estimation of the *Gaia* radial velocity accuracy as a function of sky coordinates involves many more cells (i.e. 768) than the previous diagnostics. XHIP was therefore combined with the other five ground-based catalogues to increase the global statistics, but also because it provides a full sky coverage. To test how variations in the XHIP velocity zero-points could affect the assessment of *Gaia* DR2 spatial systematics, the same diagnostics was run without the XHIP dataset. This resulted in a very similar sky pattern and statistics (minimum value, 2nd and 98th percentiles, and maximum value of the distribution −0.86, −0.38, +0.35, and +1.23 km s^{-1}, respectively), but ~10% of the sky with fewer than five stars per pixel and therefore without a calculated median.

5.2.8. Accuracy: summary

The main systematic found in the *Gaia* DR2 radial velocities is a trend with magnitude that starts around $G_{\rm RVS}$ ~9–10 mag and reaches about +500 m s^{-1} at $G^{\rm ext}_{\rm RVS} = 11.75$ mag (see Sect. 5.2.2). In addition to this trend, *Gaia* DR2 shows offsets of about +250/+300 m s^{-1} with respect to the SIM and RAVE validation samples. Other offsets, specific to a range of parameter and to a catalogue, have been identified (see previous sections for the details). They do not exceed a few 100 m s^{-1}.

5.3. Radial velocity precision

Two different datasets and statistical estimators are used to assess the precision of the *Gaia* DR2 radial velocities. The first dataset is made of a compilation of three ground-based catalogues, CU6GB, SIM, and APOGEE (the latter restricted to the stars with $G^{\rm ext}_{\rm RVS} > 8.5$ mag), which have better internal precisions than *Gaia* DR2 (see Sect. 5.3.2). Since the different catalogues have small relative offsets, they were first corrected for their median radial velocity residuals (−0.012, +0.264, and +0.268 km s^{-1} for the CU6GB, SIM, and APOGEE datasets, respectively) before being combined into a single dataset, hereafter referred to as the GB[5] validation dataset. It consists of 12 119 stars.

With this dataset, the *Gaia* DR2 radial velocity precision is calculated as the robust dispersion of the radial velocity residuals:

$$\sigma^{\rm GB}_{V_{\rm R}} = \frac{{\rm Per}(V^{\rm res}_{\rm R}, 84.15) - {\rm Per}(V^{\rm res}_{\rm R}, 15.85)}{2}, \tag{4}$$

where ${\rm Per}(V^{\rm res}_{\rm R}, 15.85)$ and ${\rm Per}(V^{\rm res}_{\rm R}, 84.15)$ are the 15.85th and 84.15th percentiles of the distribution of radial velocity residuals, respectively: $V^{\rm res}_{\rm R} = V^{\rm GDR2}_{\rm R} - V^{\rm GB}_{\rm R}$. The lower and upper 1σ uncertainties on the precision are calculated as

$$\epsilon^{\rm low}_{\sigma^{\rm GB}_{V_{\rm R}}} = \frac{\sqrt{2\pi}}{e^{-0.5}}\sqrt{\frac{0.1585 \times 0.683}{N_{V^{\rm res}_{\rm R}}}}(\tilde{V}^{\rm res}_{\rm R} - {\rm Per}(V^{\rm res}_{\rm R}, 15.85)), \tag{5}$$

$$\epsilon^{\rm upp}_{\sigma^{\rm GB}_{V_{\rm R}}} = \frac{\sqrt{2\pi}}{e^{-0.5}}\sqrt{\frac{0.1585 \times 0.683}{N_{V^{\rm res}_{\rm R}}}}({\rm Per}(V^{\rm res}_{\rm R}, 84.15) - \tilde{V}^{\rm res}_{\rm R}), \tag{6}$$

where $\tilde{V}^{\rm res}_{\rm R}$ is the median of the radial velocity residuals and $N_{V^{\rm res}_{\rm R}}$ is the number of radial velocity residuals.

The second dataset is made of all the stars with a radial velocity published in *Gaia* DR2 and is hereafter referred to as the full dataset. With this dataset, the estimator of the precision is the median of the radial velocity uncertainties (Sect. 5.1.2):

$$\sigma^{\rm Full}_{V_{\rm R}} = \tilde{\epsilon}_{V_{\rm R}}, \tag{7}$$

and the lower and upper 1σ uncertainties on the precision are calculated as

$$\epsilon^{\rm low}_{\sigma^{\rm Full}_{V_{\rm R}}} = \sqrt{\frac{\pi}{2N_{\epsilon_{V_{\rm R}}}}}(\tilde{\epsilon}_{V_{\rm R}} - {\rm Per}(\epsilon_{V_{\rm R}}, 15.85)), \tag{8}$$

$$\epsilon^{\rm upp}_{\sigma^{\rm Full}_{V_{\rm R}}} = \sqrt{\frac{\pi}{2N_{\epsilon_{V_{\rm R}}}}}({\rm Per}(\epsilon_{V_{\rm R}}, 84.15) - \tilde{\epsilon}_{V_{\rm R}}), \tag{9}$$

where $N_{\epsilon_{V_{\rm R}}}$ is the number of individual radial velocity uncertainties and $\tilde{\epsilon}_{V_{\rm R}}$, ${\rm Per}(\epsilon_{V_{\rm R}}, 15.85)$, and ${\rm Per}(\epsilon_{V_{\rm R}}, 84.15)$ are the median, 15.85th, and 84.15th percentiles, respectively, of the distribution of radial velocity uncertainties. The radial velocity uncertainty, $\epsilon_{V_{\rm R}}$, is a function of the standard deviation of the time series of transit radial velocities (see Eq. (1)). The precision derived from the full validation dataset is therefore proportional to the scatter of the transit radial velocities.

Although the full dataset is made of the 7.2 million stars, the effective temperature, surface gravity, and metallicity are known for only 1.3, 0.4, and 0.4 million stars (from a compilation of

---

[5] Standing for ground-based.

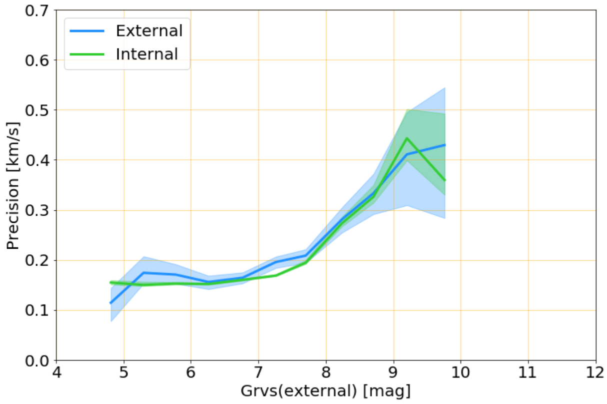

Fig. 16. Comparison of the external and internal precisions estimated using Eqs. (4) and (7), respectively, as a function of $G_{\rm RVS}^{\rm ext}$ magnitude for the CU6GB validation stars.

ground-based catalogues), respectively. The assessment of the radial velocity precision as a function of these parameters is therefore limited to these sub-samples.

The two validation datasets and the two estimators of the precision are complementary because they are sensitive to different aspects. The stars in the GB dataset have been selected on the basis of multiple ground-based observations to be as clean as possible of radial velocity variables. The full dataset contains all the 7 224 631 stars of the *Gaia* DR2 spectroscopic catalogue, which includes a proportion of undetected multiple and variable stars, even if the filters applied on the suspected SB2 and on the radial velocity uncertainty (Sect. 4) should have removed the bulk of the large amplitude velocity variables. The GB precision will account for some potential differential effects, such as the possible systematic offset between giant and dwarf stars. The full dataset precision, which relies on the scatter of the transit radial velocities of each source, is not sensitive to the possible systematics between different groups of sources.

The GB dataset is only made of 12 119 stars. Together with the full dataset, it is used to assess the precision as a function of magnitude (Sect. 5.3.2). The GB dataset is too small to assess the precision as a function of two parameters simultaneously. When the precision is assessed as a function of magnitude and number of transits (Sect. 5.3.3), magnitude and effective temperature (Sect. 5.3.4), magnitude and surface gravity (Sect. 5.3.5) or magnitude and metallicity (Sect. 5.3.6), only the full sample is therefore used.

5.3.1. Comparing the precision estimators

To compare the estimates of the precision derived with the robust dispersion of the residuals (Eq. (4)) on the one hand and with the median of the radial velocity uncertainties (Eq. (7)) on the other hand, both estimators were applied to the same subset of CU6GB stars. Figure 16 shows the external (relying on the residuals) and internal (relying on the uncertainties) precisions as a function of $G_{\rm RVS}^{\rm ext}$ magnitude. Within the uncertainties, the two estimators of the precision agree well.

5.3.2. Precision versus magnitude

Figure 17 (top) shows the robust dispersion of the radial velocity residuals (Eq. (4)) as a function of the external $G_{\rm RVS}^{\rm ext}$ magnitude for *Gaia* DR2 versus the CU6GB, SIM, RAVE, APOGEE, and GB validation datasets. The typical uncertainties of the CU6GB and SIM datasets are on the order of a few 10 m s^{-1} (Soubiran et al. 2018; Makarov & Unwin 2015). This is significantly smaller than the radial velocity residuals derived when *Gaia* DR2 was compared to these two datasets. Their uncertainties only contribute to a few percent of the measured residuals, which could therefore be used as an estimate of the *Gaia* DR2 precision. For $G_{\rm RVS}^{\rm ext} \in \sim [8.5, 11]$ mag, the residuals of *Gaia* DR2 versus CU6GB are very similar to those versus APOGEE. This indicates that the APOGEE uncertainties contribute very little to the derived residuals. For $G_{\rm RVS}^{\rm ext} \lesssim 8.5$ mag, the *Gaia* DR2-APOGEE residuals reach a plateau, which is indicative of a more significant contribution of APOGEE uncertainties to the residuals. As a consequence, only APOGEE stars fainter than $G_{\rm RVS}^{\rm ext} = 8.5$ mag were included in the GB dataset (see Sect. 5.3). The residuals with respect to the RAVE dataset include a significant contribution of RAVE uncertainties, which is why the RAVE stars were not included in the GB dataset.

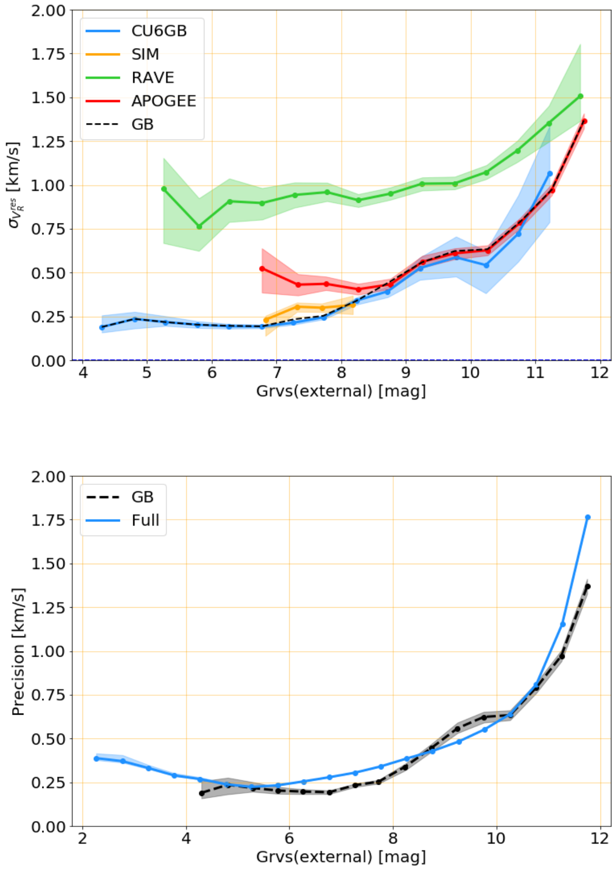

Fig. 17. *Top panel*: robust dispersion of the radial velocity residuals as a function of the external $G_{\rm RVS}^{\rm ext}$ magnitude for *Gaia* DR2 versus the CU6GB, SIM, RAVE, APOGEE, and GB validation datasets. *Bottom panel*: comparison of the precisions as a function of $G_{\rm RVS}^{\rm ext}$ magnitude, estimated with the GB dataset (dashed black line) and the full dataset (blue line). The lower and upper 1σ uncertainties on the measures of the robust dispersion are represented as shaded areas.

Figure 17 (bottom) compares the *Gaia* DR2 radial velocity precisions as a function of the external $G_{\rm RVS}^{\rm ext}$ magnitude, estimated with the GB dataset and the full dataset. The precision derived using the CU6GB sample reaches ~200–250 m s^{-1} for the stars with $G_{\rm RVS}^{\rm ext} \in [4, 8]$ mag, which is close to the precision obtained with the full dataset: ~220–350 m s^{-1}. This is about three to five times more precise than the pre-launch

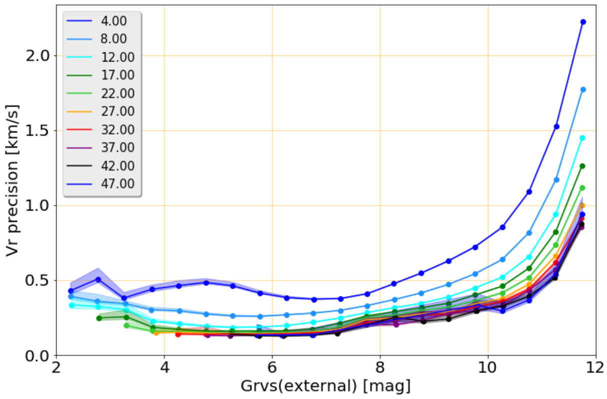

Fig. 18. Radial velocity precision as a function of $G_{\rm RVS}^{\rm ext}$ magnitude and number of transits. Each curve corresponds to an interval of five transits: for instance, [2, 6] transits (dark blue), [7, 11] transits (blue). The mean number of transits of each interval is given in the legend. The lower and upper 1σ uncertainties on the measures of the precision are represented as shaded areas.

specification, which was 1 km s^{-1}. In this range of magnitude, the *Gaia* DR2 radial velocity precision is limited by the precision of the calibrations and in particular of the wavelength calibration. From $G_{\rm RVS}^{\rm ext}$ ~ 5 mag, some spectra begin to be partially saturated. The saturation increases with decreasing magnitude, and as a consequence, the radial velocity precision deteriorates. At $G_{\rm RVS}^{\rm ext} = 11.75$ mag, the GB dataset yields a *Gaia* DR2 precision of ~1.4 km s^{-1}. The precision derived with the full sample is slightly lower, 1.8 km s^{-1}, probably because of the larger portion of unfiltered radial velocity variables.

5.3.3. Precision versus magnitude and number of transits

Figure 18 presents the radial velocity precision as a function of $G_{\rm RVS}^{\rm ext}$ magnitude and number of transits (the different curves), estimated with the full validation dataset. As expected, the precision improves with the number of transits. For example, at $G_{\rm RVS}^{\rm ext} = 11.75$ mag, the precision improves from ~2.2 to ~0.9 km s^{-1}, between 4 (dark blue line) and 37 transits (purple line).

5.3.4. Precision versus magnitude and effective temperature

Figure 19 (top left) presents the *Gaia* DR2 precision as a function of the external $G_{\rm RVS}^{\rm ext}$ magnitude and effective temperature (the different curves), assessed using the 1.3 million stars from the full dataset with known $T_{\rm eff}$. The radial velocity precision improves as the effective temperature decreases. This is the direct consequence of the evolution of the morphology of the spectra with temperature. As it decreases, the weak neutral lines on average become stronger, carrying more information to derive the radial velocity. This is illustrated in Fig. 20, which compares the spectra of HIP46933 ($T_{\rm eff} = 4487$ K, $\log g = 4.22$, [Fe/H] = −0.24 dex; Adibekyan et al. 2012) and HIP84551 ($T_{\rm eff} = 6517$ K, $\log g = 4.20$, [Fe/H] = +0.18 dex; Adibekyan et al. 2012). At $G_{\rm RVS}^{\rm ext} = 11.75$ mag, the precision is ~2.5 km s^{-1} at $T_{\rm eff}$ ~ 6650 K, ~1.5 km s^{-1} at $T_{\rm eff}$ ~ 5800 K and ~1.1 km s^{-1} at $T_{\rm eff}$ ~ 3900 K.

The top right frame in Fig. 19 is similar to the top left frame, with the curves corresponding to different interval of effective temperatures of the templates used to process the stars (rather than intervals of stellar effective temperature). Globally, the precision improves as the effective temperature of the template decreases. Locally, some adjacent curves could show the opposite behaviour. For example, a better precision is obtained for the stars that are processed with a $T_{\rm eff}^{\rm tpl} = 6750$ K template (red curve) than those that are processed with a $T_{\rm eff}^{\rm tpl} = 6500$ K template (orange curve). The sub-library used by the software module *determineAP* includes a synthetic spectrum with $T_{\rm eff}^{\rm tpl} = 6500$ K, but none with $T_{\rm eff}^{\rm tpl} = 6750$ K. For stars that were processed with a $T_{\rm eff}^{\rm tpl} = 6750$ K template, the atmospheric parameters were therefore included in the compilation of ground-based catalogues. Stars processed with a $T_{\rm eff}^{\rm tpl} = 6500$ K template are in majority not included in the ground-based compilation, and their templates were selected by *determineAP*. The stars whose templates were selected by *determineAP* suffer from a larger template mismatch than those included in the ground-based compilation, which explains the swapping of some curves. At $G_{\rm RVS}^{\rm ext} = 11.75$ mag, the precision is ~3.7 km s^{-1} at $T_{\rm eff}^{\rm tpl}$ ~ 6500 K, ~2.6 km s^{-1} at $T_{\rm eff}^{\rm tpl}$ ~ 6750 K, ~1.5 km s^{-1} at $T_{\rm eff}^{\rm tpl}$ ~ 5750 K, ~1.4 km s^{-1} at $T_{\rm eff}^{\rm tpl}$ ~ 5000 K and ~1.1 km s^{-1} at $T_{\rm eff}^{\rm tpl}$ ~ 3900 K.

The precision as a function of effective temperature (Fig. 19 top left) is representative of the performance achieved for the 1.3 million stars with known ground-based effective temperature and therefore with the smallest template mismatches. The precision as a function of the template effective temperature (Fig. 19 top right) is representative of the full 7.2 million *Gaia* DR2 stars and accounts for the full variety of template mismatches. The faint star precisions as a function of magnitude and effective temperatures quoted in the abstract and conclusion are therefore those estimated using the full sample split by template effective temperature range, which are more representative of the *Gaia* DR2 radial velocities as a whole.

5.3.5. Precision versus magnitude and surface gravity

As shown in the middle row of Fig. 19, at the faint end, the radial velocity precision improves overall as the stellar and template surface gravities decrease. Stars processed with a template with surface gravity $\log g = 3.5$ show a poorer performance. This is the consequence of a larger mismatch between the templates and the observed RVS spectra. The reduced library used by the software module *determineAP* includes a single synthetic spectrum with $T_{\rm eff}^{\rm tpl} = 6000$ and a single spectrum with 6500 K, which both have a surface gravity of 3.5. The restricted library also contains two solar metallicity templates with an effective temperature of 5500 K and surface gravities of 3.5 and 4.5. As discussed in Sect. 5.3.4, stars processed with templates that were selected in the restricted library of 28 synthetic spectra usually suffer from a larger template mismatch (and therefore a poorer radial velocity precision) than the stars with stellar parameters contained in the ground-based compilation.

5.3.6. Precision versus magnitude and metallicity

Figure 19 (bottom left) presents the radial velocity precision as a function of the external $G_{\rm RVS}^{\rm ext}$ magnitude and metallicity (the different curves) estimated using the full dataset. As expected, with increasing metallicity, the metallic lines become stronger and the radial velocity precision improves. Over the metallicity range probed in Fig. 19 (bottom left), that is, approximately [−2.0, 0.5] dex, however, the precision is only weakly sensitive to metallicity (e.g. compared to the sensitivity to temperature).

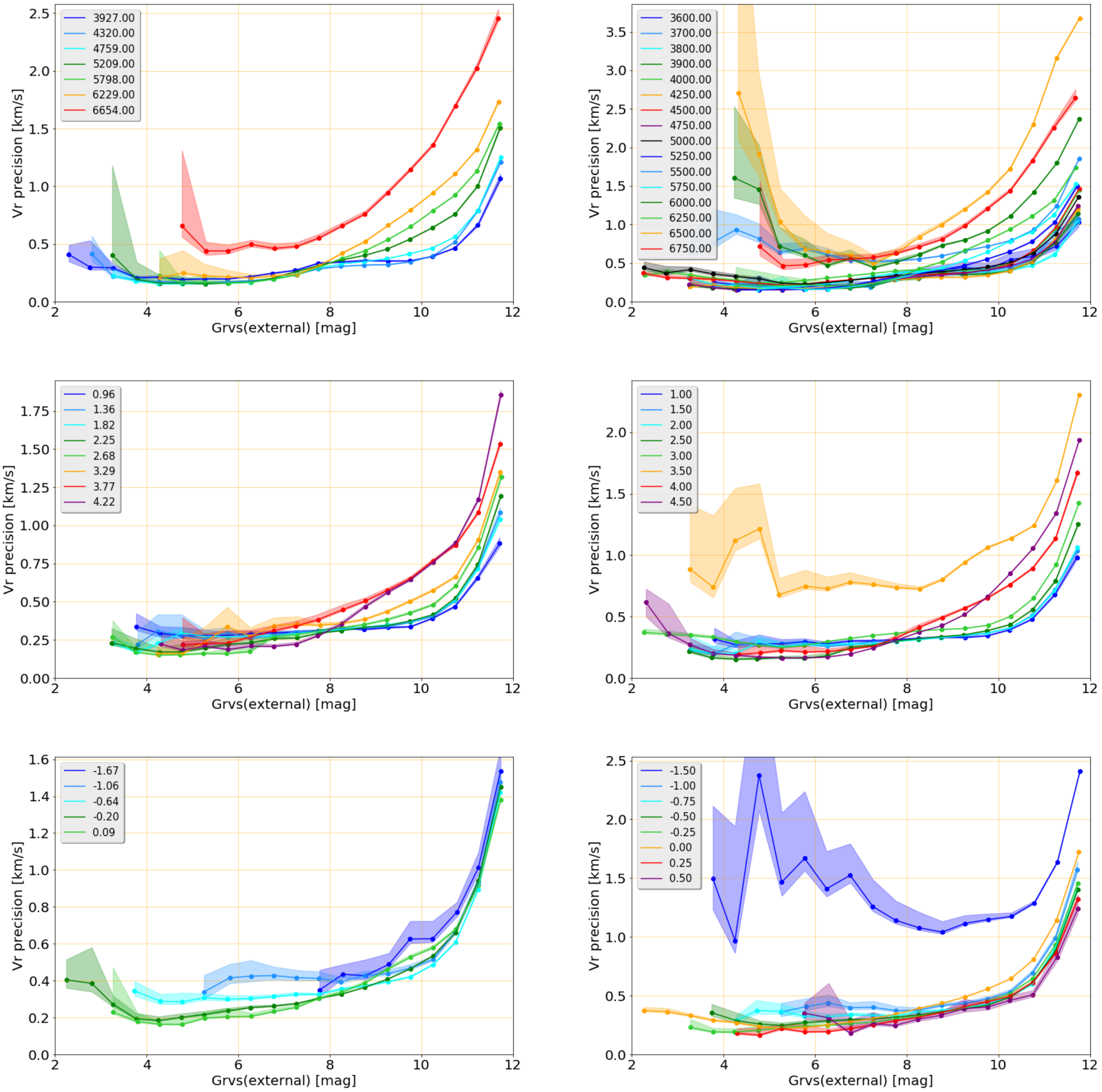

Fig. 19. *Top left panel*: radial velocity precision as a function of $G_{\rm RVS}^{\rm ext}$ magnitude and effective temperature. Each curve corresponds to an interval of 500 K: for instance, [3500, 4000] K (dark blue), [4000, 4500] K (blue). The mean effective temperature of each interval is given in the legend. *Top right panel*: radial velocity precision as a function of $G_{\rm RVS}^{\rm ext}$ magnitude and template effective temperature. Each curve corresponds to the effective temperature of a node in the grid of templates used by the spectroscopic pipeline to derive the radial velocities. The effective temperatures of the nodes are given in the legend. *Middle left panel*: radial velocity precision as a function of $G_{\rm RVS}^{\rm ext}$ magnitude and surface gravity. Each curve corresponds to an interval of 0.5 in surface gravity: for instance, [0.5, 1.0] (dark blue), [1.0, 1.5] (blue). The mean surface gravity of each interval is given in the legend. *Middle right panel*: radial velocity precision as a function of $G_{\rm RVS}^{\rm ext}$ magnitude and template surface gravity. Each curve corresponds to the surface gravity of a node in the grid of templates used by the spectroscopic pipeline to derive the radial velocities. The surface gravities of the nodes are given in the legend. *Bottom left panel*: radial velocity precision as a function of $G_{\rm RVS}^{\rm ext}$ magnitude and metallicity. Each curve corresponds to an interval of 0.5 dex: for instance, [−2.0, −1.5] dex (dark blue), [−1.5, −1.0] dex (blue). The mean metallicity of each interval is given in the legend. *Bottom right panel*: radial velocity precision as a function of $G_{\rm RVS}^{\rm ext}$ magnitude and template metallicity. Each curve corresponds to the metallicity of a node in the grid of templates used by the spectroscopic pipeline to derive the radial velocities. The metallicities of the nodes are given in the legend. The lower and upper 1σ uncertainties on the measures of the precision are represented as shaded areas.

The limited number of very metal-poor stars with known metallicities in our compilation of ground-based catalogues prevents us from assessing a reliable precision below $[{\rm Fe/H}] = -2$ dex. Figure 21 shows the individual radial velocity residuals of the CU6GB, SIM, RAVE, APOGEE, and GES validation stars. Stars more metal-poor than −2 dex mostly show (absolute) residuals lower than 4 km s^{-1}. Figure 22 shows the RVS spectrum of the metal-poor star HD 122563: $T_{\rm eff} = 4608$ K, $\log g = 1.61$, and $[{\rm Fe/H}] = -2.64$ dex (Jofré et al. 2014). Even at this very low metallicity, the ionised calcium lines are still well visible and allow deriving precise radial velocities.

Figure 19 (bottom right) presents the radial velocity precision as a function of the external $G_{\rm RVS}^{\rm ext}$ magnitude and metallicity of the template (the different curves) estimated with the full

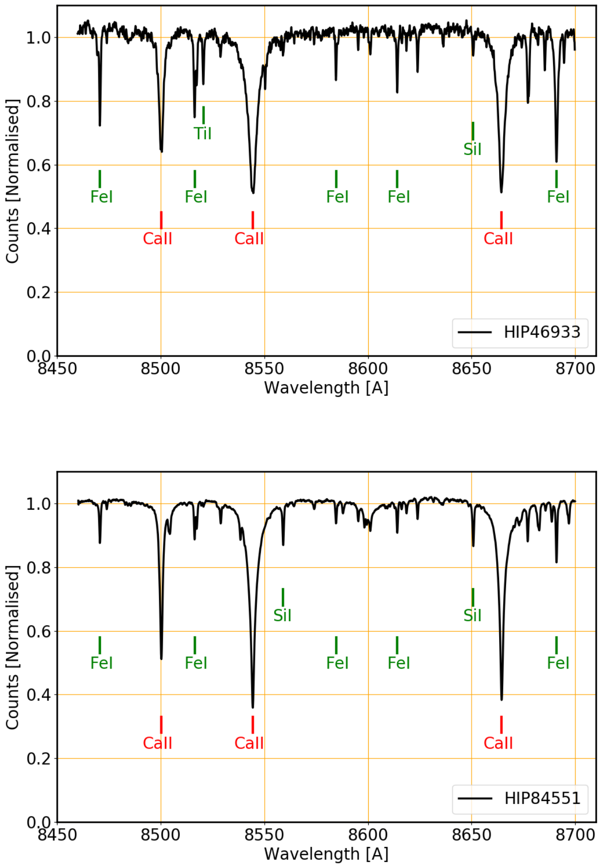

Fig. 20. Comparison of the RVS spectra of HIP46933 and HIP84551. The weak neutral lines are on average stronger in the former, which is cooler, $T_{\rm eff} = 4487$ K, than in the latter, $T_{\rm eff} = 6517$ K, and therefore allow us to derive radial velocities with higher precision (at similar $G_{\rm RVS}$ magnitude).

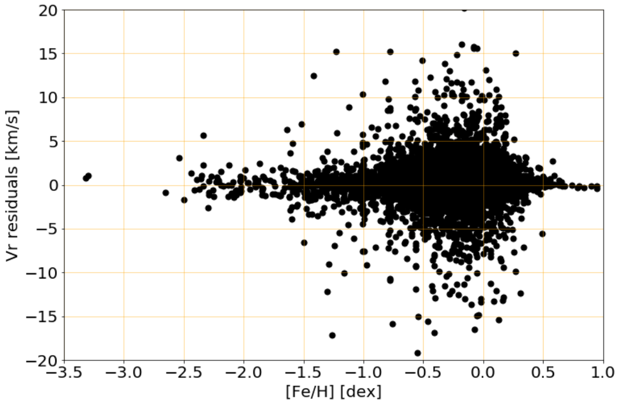

Fig. 21. Radial velocity residuals versus metallicity for the CU6GB, SIM, RAVE, APOGEE, and GES validation stars.

dataset. The reduced library of synthetic spectra used by the software module *determineAP* has two metallicities: −1.5 dex and solar. The stars processed with these two templates suffer, on average, from a stronger template mismatch than the stars processed with the other templates, which were selected using the parameters from the compilation of ground-based catalogues. As a consequence, stars processed with −1.5 dex or solar metallicity templates perform less well.

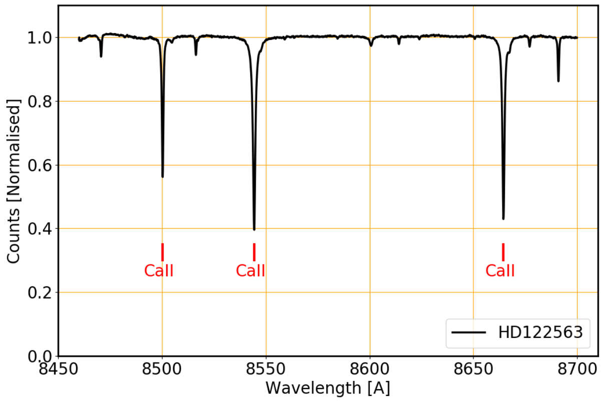

Fig. 22. RVS spectrum of the metal-poor star HD 122563, which has a metallicity [Fe/H] = −2.64 dex (Jofré et al. 2014). At this metallicity, the ionised calcium triplet is still well visible.

5.3.7. Template selection in future *Gaia* releases

In *Gaia* DR2, the 280 million spectra to process, the available processing power, and the tight processing schedule have imposed a limit of 28 spectra to the library of templates used by the software module *determineAP*. In the subsequent *Gaia* releases, the elaborated analysis of Bp, Rp, and RVS spectra (for the brightest stars) should provide precise atmospheric parameters for most RVS stars (Bailer-Jones et al. 2013; Recio-Blanco et al. 2016). The spectroscopic pipeline will rely less and less on the module *determineAP* and its limited choice of templates. An increasing fraction of the templates will be selected in the full library of 5256 synthetic spectra using *Gaia* DR3 and *Gaia* DR4 atmospheric parameters. This will reduce the mismatch between templates and observed spectra and will improve the radial velocity performance.

5.3.8. Precision versus sky coordinates

Figure 23 presents the sky map in Galactic coordinates of the radial velocity precision estimated with the full dataset for pixels of 0.2 square degree. The 2nd and 98th percentiles of the distribution are 0.53 and 2.08 km s^{-1}, while the minimum and maximum are 0.18 and 9.54 km s^{-1}. Comparison with Fig. 9 (bottom) shows that the best precisions are obtained in the areas that were repeatedly scanned by the satellite and where many spectra were recorded per source.

5.3.9. Open clusters

Open clusters are essential targets for evaluating both the consistency of radial velocities among members and the RVS zero-point by comparison to the literature. The Hyades and Pleiades are particularly well suited for that purpose because they have nearly 200 members that each have a *Gaia* DR2 radial velocity, and they have also been well studied with high-resolution spectroscopy. The radial velocity distribution of the astrometric members (Gaia Collaboration 2018b) as a function of *G* magnitude (Fig. 24) shows a high consistency of the radial velocities in a wide magnitude range, and only the dispersion increases at faint magnitude. The mean radial velocities of the Hyades and Pleiades are 39.9 ± 0.05 and 5.55 ± 0.10 km s^{-1}, respectively, with a standard deviation of ∼2 km s^{-1}, according to Gaia Collaboration (2018b), to be compared to 39.29 ± 0.25 and 5.94 ± 0.08 km s^{-1} reported by Mermilliod et al. (2009).

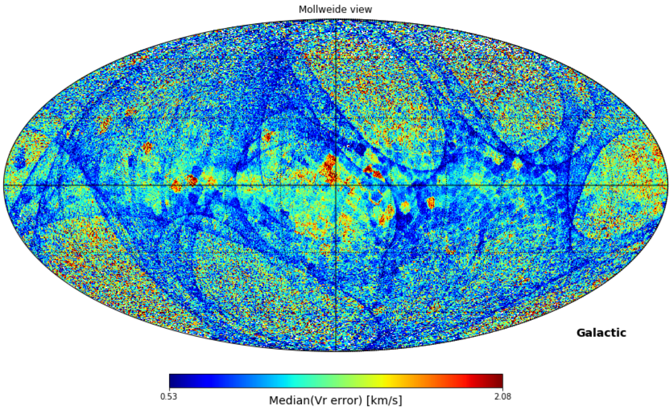

Fig. 23. Map of the radial velocity precision in Galactic coordinates. The Galactic centre is in the middle of the figure and the Galactic longitudes increase to the left. The pixel size is 0.2 square degree (healpix level 7).

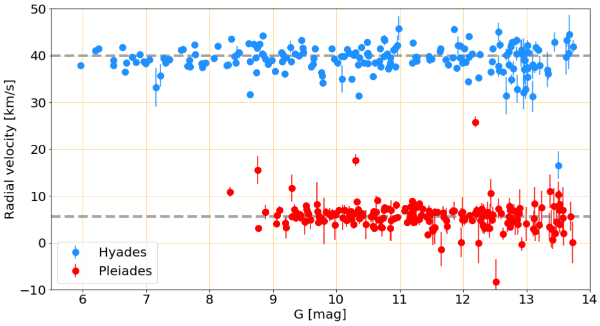

Fig. 24. *Gaia* radial velocities for the astrometric members of the Hyades and Pleiades provided by Gaia Collaboration (2018b) as a result of their membership analysis of nearby open clusters. Each of these two clusters has almost 200 stars with a *Gaia* radial velocity. The grey lines indicate the weighted averages of the radial velocity that result from the analysis performed by Gaia Collaboration (2018b). The dispersion around the mean is ~2 km s^{-1}.

Other open clusters can be used for comparison to the literature based on astrometric membership established by Gaia Collaboration (2018b) and Arenou et al. (2018). The weighted mean radial velocity has been determined for open clusters with at least four *Gaia* DR2 member stars with a good radial velocity measurement (i.e. an uncertainty smaller than 5 km s^{-1}) after outliers that deviate by more than 10 km s^{-1} from the median cluster velocity were rejected. Comparison is made with radial velocities compiled in the catalogue of Dias et al. (2002), updated in 2016, excluding the clusters whose ground-based radial velocities were derived from only one or two stars, as well as the cluster NGC 6991, which is flagged "n", that is, "non-existent NGC" in Dias et al. (2002). The difference in radial velocity is shown in Fig. 25 for 63 clusters in common. Three clusters show RV differences larger than 5 km s^{-1}. For NGC 2422 and Trumpler 10, the *Gaia* DR2 radial velocities differ by ~10 km s^{-1} from the values of Dias. However, both clusters have also been studied with RAVE by Conrad et al. (2017), who determined mean radial velocities that agree well with those from *Gaia* DR2 in the two cases. Stock 12 has the largest radial velocity difference between *Gaia* and Dias with 14.3 ± 4.2 km s^{-1} based on ten stars on the *Gaia* DR2 side and four stars in Dias catalogue. No other determination exists in the literature. For the other clusters, the *Gaia* DR2 radial velocities

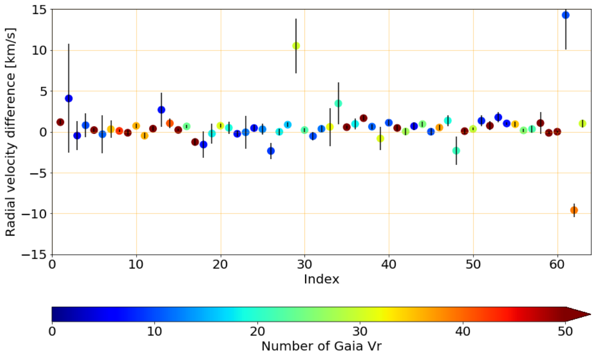

Fig. 25. Difference of mean radial velocities between *Gaia* and the literature (Dias et al. 2002) for 63 open clusters. The error bars correspond to the quadratic sum of *Gaia* and literature uncertainties. The abscissa is an arbitrary number of the clusters from 1 to 63. The colour code highlights the number of *Gaia* members per cluster, which varies from 5 to 191.

and those of the literature agree well, with a median difference of 0.4 km s^{-1} and a standard deviation of 1.1 km s^{-1}.

6. Conclusion

Gaia DR2 contains median radial velocities for 7 224 631 stars brighter than $G_{\rm RVS} = 12$ mag and with effective temperatures in the range [3550, 6900] K. These stars offer a full-sky coverage and a completeness with respect to the full second *Gaia* data release of 77.2%, for stars with $G \leq 12.5$ mag. The accuracy of the radial velocities has been assessed by comparison to several ground-based catalogues. The medians of the radial velocity residuals vary from one catalogue to another, but do not exceed a few 100 m s^{-1}. In addition, *Gaia* DR2 radial velocities present a positive trend with magnitude, starting around $G_{\rm RVS} = 9$ mag and rising up to ~500 m s^{-1} at $G_{\rm RVS} = 11.75$ mag. The origin of the trend is under investigation, with the aim to correct for it in *Gaia* DR3. The radial velocity precision has been assessed both by comparison with ground-based catalogues and using the distribution of *Gaia* radial velocity uncertainties. For bright stars with $G_{\rm RVS}$ in [4, 8] mag, the radial velocity precision, estimated using the full dataset, is in the range 220–350 m s^{-1}. At the faint end, $G_{\rm RVS} = 11.75$ mag, the precisions are 1.4 and 3.7 km s^{-1} for $T_{\rm eff} = 5000$ and 6500 K.

Beyond *Gaia* DR2, several data releases are already planned[6]. Each one should include refined data treatments, new functionalities, new products, and a fainter processing limit for the radial velocities. *Gaia* DR3 is expected to include radial velocities for stars down to $G_{\rm RVS} = 14$ mag, while *Gaia* DR4 aims at reaching the limiting magnitude of the RVS: $G_{\rm RVS} = 16.2$ mag.

Acknowledgements. This work has made use of results from the European Space Agency (ESA) space mission *Gaia*, the data from which were processed by the *Gaia* Data Processing and Analysis Consortium (DPAC). Funding for the DPAC has been provided by national institutions, in particular the institutions participating in the *Gaia* Multilateral Agreement. The *Gaia* mission website is `http://www.cosmos.esa.int/gaia`. Most of the authors are current or past members of the ESA *Gaia* mission team and of the *Gaia* DPAC and their work has been supported by the French Centre National de la Recherche Scientifique (CNRS), the Centre National d'Etudes Spatiales (CNES), the Agence Nationale de la Recherche, the Région Aquitaine, the Université de Bordeaux, the Utinam Institute of the Université de Franche-Comté, and the Institut des Sciences de l' Univers (INSU); the Science and Technology Facilities Council and the United Kingdom Space Agency; the Belgian Federal

---

[6] `https://www.cosmos.esa.int/web/gaia/release`

Science Policy Office (BELSPO) through various Programme de Développement d'Expériences Scientifiques (PRODEX) grants; the German Aerospace Agency (Deutsches Zentrum fur Luft- und Raumfahrt e.V., DLR); the Algerian Centre de Recherche en Astronomie, Astrophysique et Géophysique of Bouzareah Observatory; the Swiss State Secretariat for Education, Research, and Innovation through the ESA PRODEX programme, the Mesures d'Accompagnement, the Swiss Activités Nationales Complémentaires, and the Swiss National Science Foundation; the Slovenian Research Agency (research core funding No. P1-0188). This research has made use of the SIMBAD database (Wenger et al. 2000) developed and operated at CDS, Strasbourg, France.

References

Abolfathi, B., Aguado, D. S., Aguilar, G., et al. 2018, ApJS, 235, 42
Adibekyan, V. Z., Sousa, S. G., Santos, N. C., et al. 2012, A&A, 545, A32
Anderson, E., & Francis, C. 2012, Astron. Lett., 38, 331
Andrae, R., Fouesneau, M., Creevey, O., et al. 2018, A&A, 616, A8 (*Gaia* 2 SI)
Arenou, F., Luri, X., Babusiaux, C., et al. 2018, A&A, 616, A17 (*Gaia* 2 SI)
Bailer-Jones, C. A. L., Andrae, R., Arcay, B., et al. 2013, A&A, 559, A74
Baranne, A., Queloz, D., Mayor, M., et al. 1996, A&AS, 119, 373
Buder, S., Asplund, M., Duong, L., et al. 2018, MNRAS, 478, 4513
Conrad, C., Scholz, R. D., Kharchenko, N. V., et al. 2017, A&A, 600, A106
Cropper, M., Katz, D., Sartoretti, P., et al. 2018, A&A, 616, A5 (*Gaia* 2 SI)
Cui, X.-Q., Zhao, Y.-H., Chu, Y.-Q., et al. 2012, Res. Astron. Astrophys, 12, 1197
Dias, W. S., Alessi, B. S., Moitinho, A., & Lépine, J. R. D. 2002, A&A, 389, 871
Evans, D., Riello, M., De Angeli, F., et al. 2018, A&A, 616, A4 (*Gaia* 2 SI)
Gaia Collaboration (Prusti, T., et al.) 2016a, A&A, 595, A1
Gaia Collaboration (Brown, A. G. A., et al.) 2016b, A&A, 595, A2
Gaia Collaboration (Brown, A. G. A., et al.) 2018a, A&A, 616, A1 (*Gaia* 2 SI)
Gaia Collaboration (Babusiaux, C., et al.) 2018b, A&A, 616, A10 (*Gaia* 2 SI)
Gilmore, G., Randich, S., Asplund, M., et al. 2012, The Messenger, 147, 25
Holtzman, J. A., Shetrone, M., Johnson, J. A., et al. 2015, AJ, 150, 148
Houk, N., & Cowley, A. P. 1975, Michigan Catalogue of Two-Dimensional Spectral Types for the HD Stars. Declinations -90 to -53. (Michigan: University of Michigan)
Jackson, R. J., Jeffries, R. D., Lewis, J., et al. 2015, A&A, 580, A75
Jofré, P., Heiter, U., Soubiran, C., et al. 2014, A&A, 564, A133
Jordi, C., Gebran, M., Carrasco, J. M., et al. 2010, A&A, 523, A48
Kordopatis, G., Gilmore, G., Steinmetz, M., et al. 2013, AJ, 146, 134
Kos, J., Lin, J., Zwitter, T., et al. 2017, MNRAS, 464, 1259
Kunder, A., Kordopatis, G., Steinmetz, M., et al. 2017, AJ, 153, 75
Lindegren, L., Hernández, J., Bombrun, A., et al. 2018, A&A, 616, A2 (*Gaia* 2 SI)
Majewski, S. R., Schiavon, R. P., Frinchaboy, P. M., et al. 2017, AJ, 154, 94
Makarov, V. V., & Unwin, S. C. 2015, MNRAS, 446, 2055
Martell, S. L., Sharma, S., Buder, S., et al. 2017, MNRAS, 465, 3203
Mayor, M., Pepe, F., Queloz, D., et al. 2003, The Messenger, 114, 20
Mermilliod, J.-C., Mayor, M., & Udry, S. 2009, A&A, 498, 949
Nordström, B., Mayor, M., Andersen, J., et al. 2004, A&A, 418, 989
Perruchot, S., Kohler, D., Bouchy, F., et al. 2008, Proc. SPIE, 7014, 70140J
Queloz, D., Mayor, M., Udry, S., et al. 2001, The Messenger, 105, 1
Recio-Blanco, A., de Laverny, P., Allende Prieto, C., et al. 2016, A&A, 585, A93
Reid, M. J., Menten, K. M., Brunthaler, A., et al. 2014, ApJ, 783, 130
Riello, M., De Angeli, F., Evans, D., et al. 2018, A&A, 613, A3 (*Gaia* 2 SI)
Sacco, G. G., Morbidelli, L., Franciosini, E., et al. 2014, A&A, 565, A113
Sartoretti, P., Katz, D., Cropper, M., et al. 2018, A&A, 616, A6 (*Gaia* 2 SI)
Soubiran, C., Jasniewicz, G., Chemin, L., et al. 2018, A&A, 616, A7 (*Gaia* 2 SI)
Steinmetz, M., Zwitter, T., Siebert, A., et al. 2006, AJ, 132, 1645
Wenger, M., Ochsenbein, F., Egret, D., et al. 2000, A&AS, 143, 9
Yanny, B., Rockosi, C., Newberg, H. J., et al. 2009, AJ, 137, 4377
Zhao, G., Zhao, Y.-H., Chu, Y.-Q., Jing, Y.-P., & Deng, L.-C. 2012, Res. Astron. and Astrophys., 12, 723
Zwitter, T., Kos, J., Chiavassa, A., et al. 2018, MNRAS, 481, 645

---

[1] GEPI, Observatoire de Paris, Université PSL, CNRS, 5 Place Jules Janssen, 92190 Meudon, France
e-mail: `david.katz@obspm.fr`
[2] Mullard Space Science Laboratory, University College London, Holmbury St Mary, Dorking, Surrey RH5 6NT, UK
[3] Royal Observatory of Belgium, Ringlaan 3, 1180 Brussels, Belgium
[4] Laboratoire Univers et Particules de Montpellier, Université Montpellier, CNRS, Place Eugène Bataillon, CC72, 34095 Montpellier Cedex 05, France
[5] CNES Centre Spatial de Toulouse, 18 avenue Edouard Belin, 31401 Toulouse Cedex 9, France
[6] CRAAG – Centre de Recherche en Astronomie, Astrophysique et Géophysique, Route de l'Observatoire Bp 63 Bouzareah, 16340 Alger, Algeria
[7] Institut d'Astrophysique et de Géophysique, Université de Liège, 19c, Allée du 6 Août, 4000 Liège, Belgium
[8] Universiteit Antwerpen, Onderzoeksgroep Toegepaste Wiskunde, Middelheimlaan 1, 2020 Antwerpen, Belgium
[9] F.R.S.-FNRS, Rue d'Egmont 5, 1000 Brussels, Belgium
[10] Thales Services for CNES Centre Spatial de Toulouse, 18 avenue Edouard Belin, 31401 Toulouse Cedex 9, France
[11] Department of Astronomy, University of Geneva, Chemin d'Ecogia 16, CH-1290 Versoix, Switzerland
[12] Leibniz Institute for Astrophysics Potsdam (AIP), An der Sternwarte 16, 14482 Potsdam, Germany
[13] Laboratoire d'astrophysique de Bordeaux, Université de Bordeaux, CNRS, B18N, allée Geoffroy Saint-Hilaire, 33615 Pessac, France
[14] Laboratoire Lagrange, Université Nice Sophia-Antipolis, Observatoire de la Côte d'Azur, CNRS, CS 34229, 06304 Nice Cedex, France
[15] Instituto de Astrofísica de Canarias, 38205 La Laguna, Tenerife, Spain
[16] Universidad de La Laguna, Departamento de Astrofísica, 38206 La Laguna, Tenerife, Spain
[17] Université Grenoble Alpes, CNRS, IPAG, 38000 Grenoble, France
[18] Max Plank Institute für Sonnensystemforschung, Justus-von-Liebig-Weg 3, 37077 Göttingen, Germany
[19] Unidad de Astronomía, Fac. Cs. Básicas, Universidad de Antofagasta, Avda. U. de Antofagasta 02800, Antofagasta, Chile
[20] ATOS for CNES Centre Spatial de Toulouse, 18 avenue Edouard Belin, 31401 Toulouse Cedex 9, France
[21] Max Planck Institute for Extraterrestrial Physics, High Energy Group, Gießenbachstraße, 85741 Garching, Germany
[22] Institute for Astronomy, University of Edinburgh, Royal Observatory, Blackford Hill, Edinburgh EH9 3HJ, UK
[23] LNE-SYRTE, Observatoire de Paris, Université PSL, CNRS, Sorbonne Université, 61 avenue de l'Observatoire, 75014 Paris, France
[24] Faculty of Mathematics and Physics, University of Ljubljana, Jadranska ulica 19, 1000 Ljubljana, Slovenia
[25] INAF-Osservatorio Astronomico di Padova, vicolo Osservatorio 5, 35122 Padova, Italy
[26] INAF Astronomical Observatory of Padova, 36012 Asiago (VI), Italy
[27] Research School of Astronomy and Astrophysics, Australian National University, Canberra, ACT 2611, Australia

Appendix A: Distribution of the template parameters

Figure A.1 shows the distributions of the effective temperatures (top), surface gravities (middle), and metallicities (bottom) of the templates. The alternation of large and small peaks in the effective temperature distribution arises because certain temperatures are only chosen when the stars are contained in the ground-based catalogue compilations (producing small peaks). Similar selection effects are visible for surface gravity (few templates with $\log g \leq 2.5$ or equal to 4) and metallicity (templates mostly solar, with a "small" secondary peak at [Fe/H] = −1.5 dex, which are the metallicities in the sub-library used by the dedicated selection module).

Appendix B: Charge transfer inefficiency

As described in Sect. 5.2.2, the *Gaia* radial velocities exhibit a trend with magnitude. The first lead that was explored to explain this trend was the charge transfer inefficiency (CTI). When they hit the CCDs, high-energy particles damage the pixels, producing traps that could snare a fraction of the spectrum photoelectrons, preventing them from propagating consistently with the rest of the signal from CCD column to CCD column. Eventually, the trapped photoelectrons are released. If the release time is short (i.e. the time for the spectrum to be propagated by one or a few pixels), the CTI does not remove the signal from the spectrum, but instead distorts the line spread function (LSF) profile, producing a trail in the direction opposite to the propagation of the spectrum. In the RVS, the blue edge of the spectrum is leading. The CTI would therefore produce a tail on the LSF red edge, shifting the line centroids to higher wavelengths and applying a positive shift to the radial velocities. Pre-launch ground-based laboratory tests have shown that the impact of CTI increases as the signal decreases. We would therefore expect a positive radial velocity trend with magnitude from CTI, which is what we observe. The CTI effect is also expected to increase with time, as the radiation damages accumulate. This prediction is not verified by the *Gaia* radial velocities. The trend appears to be stable in time. The CTI therefore probably does not cause the trend.

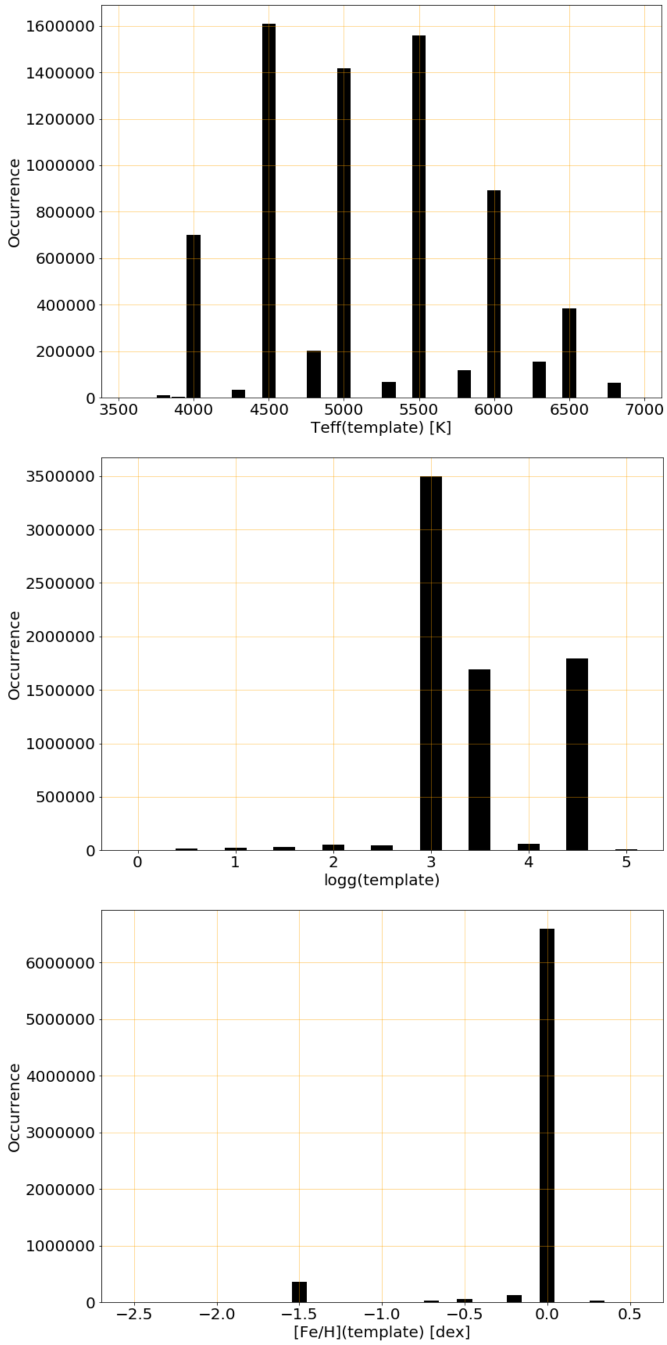

Fig. A.1. *Top panel*: distribution of the effective temperatures of the templates. *Middle panel*: distribution of the surface gravities of the templates. *Bottom panel*: distribution of the metallicities of the templates.